Surface Inorganic Iodine Speciation in the Indian and Southern Oceans from 12o N to 70o S

Rosie Chance[1], Tinel Liselotte[1], Amit Sarkar[2], Alok K Sinha[2], Anoop S Mahajan[3], Racheal Chacko[4], P Sabu[4], Rajdeep Roy[5], Tim D Jickells[6], David Stevens[7], Martin Wadley[7], and Lucy J Carpenter[8]

[1]Wolfson Atmospheric Chemistry Laboratories, Department of Chemistry, University of York, York, YO10 5DD, UK.
[2]National Centre for Polar and Ocean Research, Ministry of Earth Sciences, Goa 403804, India.
[3]Indian Institute of Tropical Meteorology, Ministry of Earth Sciences, Pune 411008, India
[4]National Centre for Polar and Ocean Research, Ministry of Earth Sciences, Goa 403804, India
[5]National Remote Sensing centre (NRSC), Indian Space Research Organisation (ISRO), Department of Space, Government of India
[6]Centre for Ocean and Atmospheric Sciences, School of Environmental Sciences, University of East Anglia, Norwich Research Park, Norwich, NR4 7TJ, UK
[7]Centre for Ocean and Atmospheric Sciences, School of Mathematics, University of East Anglia, Norwich Research Park, Norwich, NR4 7TJ, UK
[8]Wolfson Atmospheric Chemistry LaboratorieWolfson Atmospheric Chemistry Laboratories, Department of Chemistry, University of Y ork, Y ork, YO10 5DD, UK

November 21, 2022

Abstract

Marine iodine speciation has emerged as a potential tracer of primary productivity, sedimentary inputs, and ocean oxygenation. The reaction of iodide with ozone at the sea surface has also been identified as the largest deposition sink for tropospheric ozone and is also thought to be the dominant source of iodine to the atmosphere. Accurate incorporation of these processes into atmospheric models requires improved understanding of iodide concentrations at the air-sea interface. Observations of sea surface iodide are relatively sparse and are particularly lacking in the Indian Ocean basin. We present 127 new sea surface ([?]10 m depth) iodide and iodate observations made during three cruises in the Indian Ocean and the Indian sector of the Southern Ocean. The observations span latitudes from ~12oN to ~70oS, and include three distinct hydrographic regimes: the South Indian subtropical gyre, the Southern Ocean and the northern Indian Ocean including the Southern Bay of Bengal. Concentrations were broadly comparable to those observed at similar latitudes in other ocean basins. The spatial distribution of sea surface iodide follows the same general trends as in other ocean basins, with iodide concentrations tending to decrease with increasing latitude (and decreasing sea surface temperature). However, the gradient of this relationship was steeper in subtropical waters of the Indian Ocean than in the Atlantic or Pacific, suggesting that it might not be accurately represented by widely used parameterisations based on sea surface temperature. Iodide concentrations in the tropical northern Indian Ocean were higher and more variable than elsewhere. Two extremely high iodide concentrations (1241 and 949 nM) were encountered in the Bay of Bengal and are thought to be associated with sedimentary inputs under low oxygen conditions. Excluding these outliers, sea surface iodide concentrations ranged from 20 to 250 nM, with a median of 61 nM. Controls on sea surface iodide

concentrations in the Indian Ocean were investigated using a state-of-the-art iodine cycling model. Multiple interacting factors were found to drive the iodide distribution. Dilution via vertical mixing and mixed layer depth shoaling are key controls, and both also modulate the impact of biogeochemical iodide formation and loss processes.

Surface Inorganic Iodine Speciation in the Indian and Southern Oceans from 12°N to 70°S

Running title: Iodine in the Indian Ocean

Rosie J. Chance[1*+], Liselotte Tinel[1+], Amit Sarkar[2‡], Alok K. Sinha[2], Anoop S. Mahajan[3], Racheal Chacko[2], P. Sabu[2], Rajdeep Roy[4], Tim D. Jickells[5], David Stevens[6], Martin Wadley[6], Lucy J. Carpenter[1]

1. Wolfson Atmospheric Chemistry Laboratories, Department of Chemistry, University of York, York, YO10 5DD, UK.
2. National Centre for Polar and Ocean Research, Ministry of Earth Sciences, Goa 403804, India.
3. Indian Institute of Tropical Meteorology, Ministry of Earth Sciences, Pune 411008, India.
4. National Remote Sensing centre (NRSC), Indian Space Research Organisation (ISRO), Department of Space, Government of India.
5. Centre for Ocean and Atmospheric Sciences, School of Environmental Sciences, University of East Anglia, Norwich Research Park, Norwich, NR4 7TJ, UK.
6. Centre for Ocean and Atmospheric Sciences, School of Mathematics, University of East Anglia, Norwich Research Park, Norwich, NR4 7TJ, UK.

+ Authors contributed equally to this manuscript

Current address:
‡ Ecosystem based management of marine resources, (EBMMR), Environment and Life Sciences Research Center, Kuwait Institute for Scientific Research, Salmiya, Kuwait

* Correspondence: Corresponding author rosie.chance@york.ac.uk

Key words: iodine, iodide, iodate, seawater, Indian Ocean, Southern Ocean

Contribution to the Field

The presence of iodide-iodine at the ocean surface impacts air quality and climate. Specifically, the reaction of iodide with ozone at the sea surface is the dominant source of iodine to the atmosphere, and a significant sink for tropospheric (pollutant) ozone. In the atmosphere, iodine takes part in further reactions which remove more ozone, affect greenhouse gas lifetimes and contribute to particle formation. The rate of ozone removal and iodine emission depends on the sea surface iodide concentration, but iodide measurements are sparse and have hitherto been almost completely lacking in the Indian Ocean basin. Here we present an extensive new set of sea-surface iodide measurements, spanning latitudes from ~12°N to ~70°S and including measurements from the Bay of Bengal, the Arabian Sea, the open Indian Ocean and the Indian Ocean sector of the Southern Ocean. This data set represents a substantial increase in the global coverage of sea surface iodide observations. It will help improve our understanding of marine iodine biogeochemistry, and our ability to predict the impact of iodine chemistry on the atmosphere. We compare the observed distribution to that in other ocean basins, and explore the drivers of the distribution using an ocean iodine cycling model.

Abstract

Marine iodine speciation has emerged as a potential tracer of primary productivity, sedimentary inputs, and ocean oxygenation. The reaction of iodide with ozone at the sea surface has also been identified as the largest deposition sink for tropospheric ozone and is also thought to be the dominant source of iodine to the atmosphere. Accurate incorporation of these processes into atmospheric models requires improved understanding of iodide concentrations at the air-sea interface. Observations of sea surface iodide are relatively sparse and are particularly lacking in the Indian Ocean basin. We present 127 new sea surface ($\leq$10 m depth) iodide and iodate observations made during three cruises in the Indian Ocean and the Indian sector of the Southern Ocean. The observations span latitudes from ~12$\circ$N to ~70$\circ$S, and include three distinct hydrographic regimes: the South Indian subtropical gyre, the Southern Ocean and the northern Indian Ocean including the Southern Bay of Bengal. Concentrations were broadly comparable to those observed at similar latitudes in other ocean basins. The spatial distribution of sea surface iodide follows the same general trends as in other ocean basins, with iodide concentrations tending to decrease with increasing latitude (and decreasing sea surface temperature). However, the gradient of this relationship was steeper in subtropical waters of the Indian Ocean than in the Atlantic or Pacific, suggesting that it might not be accurately represented by widely used parameterisations based on sea surface temperature. Iodide concentrations in the tropical northern Indian Ocean were higher and more variable than elsewhere. Two extremely high iodide concentrations (1241 and 949 nM) were encountered in the Bay of Bengal and are thought to be associated with sedimentary inputs under low oxygen conditions. Excluding these outliers, sea surface iodide concentrations ranged from 20 to 250 nM, with a median of 61 nM. Controls on sea surface iodide concentrations in the Indian Ocean were investigated using a state-of-the-art iodine cycling model. Multiple interacting factors were found to drive the iodide distribution. Dilution via vertical mixing and mixed layer depth shoaling are key controls, and both also modulate the impact of biogeochemical iodide formation and loss processes.

Introduction

Iodine is naturally present in the ocean, predominantly as the inorganic ions iodide (I$^-$) and iodate (IO$_3^-$). Iodine speciation is linked to many aspects of ocean biogeochemistry, and has been proposed as a tracer of primary productivity (Ducklow et al. 2018; Wong 2001), sedimentary inputs and oxygen status (Lu et al. 2018; Moriyasu et al. 2020). In addition, the concentration of iodide at the sea surface has recently attracted renewed interest from atmospheric chemists because of its impact on atmospheric composition and air quality e.g. (Sherwen et al. 2017; Cuevas et al. 2018). Specifically, the heterogeneous reaction of iodide with ozone at the sea surface has been identified as the largest, but also most uncertain, deposition sink for tropospheric ozone (Hardacre, Wild, and Emberson 2015), and the dominant source of volatile reactive iodine (as I$_2$ and HOI) to the lower atmosphere (Carpenter et al. 2013). Following emission from the ocean, reactive iodine species initiate catalytic ozone depletion cycles, and hence further influence the oxidative capacity of the atmosphere. Atmospheric iodine cycling results in the formation of iodide oxides, which have been implicated in the nucleation of particles in coastal marine areas (McFiggans et al. 2004; Allan et al. 2015).In remote marine locations, iodine chemistry may also indirectly contribute to the depletion of inorganic volatile species such as gaseous elemental mercury during the polar spring (Wang et al. 2014). The ozone-iodide reaction is now thought to be the dominant source of iodine to the atmosphere, with other sources (e.g. release of iodinated organic compounds by marine algae) contributing only around 20% of the total iodine flux to the atmosphere globally (Carpenter et al. 2013; Prados-Roman et al. 2015). To incorporate the sea surface ozone sink and/or iodine source into atmospheric models, iodide concentrations at the interface need to be predicted accurately. However, parameterizations for global sea surface iodide concentrations (MacDonald et al. 2014; Chance et al. 2014) have been limited by the relative scarcity of observations. This is particularly the case for the Indian Ocean basin, where only a few sea surface iodide observations have hitherto been reported (Chance et al. 2014), but atmospheric iodine chemistry has been investigated (e.g. (Mahajan et al. 2019).

In ocean waters, total inorganic iodine concentrations (the sum of iodide and iodate) behave approximately conservatively, with a value of around 450-500 nM across most of the oceans e.g. (Elderfield and Truesdale 1980; Truesdale, Bale, and Woodward 2000). Iodate is thermodynamically the more stable form under oxygenated conditions, and hence is present at higher concentrations throughout most ocean depths. However, at the ocean surface iodide concentrations are elevated and iodate depleted, despite this being thermodynamically unfavourable. Sea surface iodide concentrations typically range from undetectable to ~250 nM, with values higher than this only encountered as outliers (Chance et al. 2014). Iodide concentrations and the iodide to iodate ratio decline with depth below the euphotic zone, and iodide concentrations are generally very low (<20 nM) in oxygenated waters below ~500 m e.g.(Waite, Truesdale, and Olafsson 2006; Nakayama et al. 1989; Bluhm et al. 2011). The ratio of iodide to iodate varies with location as well as depth. Sea surface iodide concentrations exhibit a pronounced latitudinal gradient, with highest surface iodide concentrations observed at low latitudes and in coastal waters (Chance et al. 2014). In addition to these two inorganic forms, iodine also occurs in seawater associated with dissolved organic matter as so-called dissolved organic iodine (DOI; e.g. (Wong and Cheng 1998)). Organic forms of iodine are abundant in estuarine environments, where they can represent up to 64% of the total iodine (Wong and Cheng 1998; Schwehr and Santschi 2003). In the open ocean, levels of DOI are typically low (<5 % of the total iodine), but higher levels (e.g. 22% of total iodine) have sometimes been encountered (Wong and Cheng 1998).

130
131 The distribution of iodine species in the oceans is thought to result from a combination of
132 hydrodynamic and biogeochemical drivers, which are not yet fully understood (Chance et al.
133 2014). The formation of iodide from iodate in the euphotic zone is thought to be associated
134 with primary productivity, but the exact mechanism by which this occurs is not yet known
135 (Chance et al. 2010; Campos et al. 1996; Bluhm et al. 2010). Similarly, the route for iodide
136 oxidation back to iodate has been elusive, although recent work has suggested it may be
137 linked to bacterial nitrification (Zic, Caric, and Ciglenecki 2013; Hughes et al. 2020). The
138 lifetime of iodide with respect to oxidation is poorly constrained but thought to be relatively
139 long, with estimates ranging from several months (Campos et al. 1996; Zic, Caric, and
140 Ciglenecki 2013) or more (Hardisty et al. 2020), to as much as 40 years (Tsunogai 1971;
141 Edwards and Truesdale 1997). Given the relatively long lifetime of iodide in seawater, its
142 distribution is also strongly influenced by advection and vertical mixing e.g. (Campos et al.
143 1996; Truesdale, Bale, and Woodward 2000). The interplay of these driving factors results in
144 global scale correlations between sea-surface iodide concentrations and sea-surface
145 temperature (SST), and nitrate (Chance et al. 2014), which have been used to predict sea-
146 surface iodide fields e.g. (Ganzeveld et al. 2009; MacDonald et al. 2014; Sarwar et al. 2016).
147 In particular, spatial variations in ocean mixed layer depth are likely to be the primary cause
148 of the widely used relationship between sea surface iodide concentration and SST.

149
150 This manuscript explores an extensive new set of sea surface iodide and iodate observations
151 from the Indian Ocean and the Indian sector of the Southern Ocean, spanning latitudes from
152 ~12◦N to ~70◦S, regions which until now have been lacking in observations (Chance et al.
153 2014). To the best of our knowledge, only three studies have previously reported iodine
154 speciation in the Indian Ocean, and all have been in the west of the basin (East African
155 coastal area (Truesdale 1978) and Arabian Sea (Farrenkopf and Luther 2002; Farrenkopf et
156 al. 1997)). Of the data presented in these studies, there were only two sea surface iodide
157 observations - both from the Arabian Sea (see Figure 1) - that could be included in Chance et
158 al., 2014. The aim of this study was to substantially increase the number of observations in
159 this region, in order to both improve understanding of large-scale gradients in ocean iodine
160 speciation, and to increase global data coverage for model validation and the improvement of
161 ocean iodide parameterisations. All of these will contribute to the creation of more accurate
162 boundary conditions for atmospheric chemistry models.

163
164 **Materials and methods**

165
166 ***Sample collection***

167
168   *[Figure 1]*

169
170 Samples were collected during three research cruises in the Indian Ocean and Indian sector of
171 the Southern Ocean. Sampling locations for each cruise are shown in Figure 1. Samples were
172 collected from the Bay of Bengal (BoB) during a zonal section cruise (Bay of Bengal
173 Boundary Layer Experiment - BoBBLe) along 8°N, from 85.3°E to 89°E. The cruise took
174 place between 24/6/2016 and 23/7/2016, on board the RV *Sindhu Sadhana*. In the Arabian
175 Sea, samples were collected during the Rama mooring equatorial cruise IO1-16-SK (known
176 as SK333 here), operated by Ministry of Earth Sciences, India (MoES) and National Oceanic
177 and Atmospheric Administration, USA (NOAA), and taking place on the ORV *Sagar Kanya*.
178 The cruise departed Chennai, India, on 23/08/2016 and returned to Sri Lanka on 23/09/2016.
179 Samples were collected from the Southern Indian Ocean and Southern Ocean during the 9th

180 Indian Southern Ocean Expedition (SOE9; Jan-March 2017), from Mauritius (22°S) to coastal
181 waters of Prydz Bay, Antarctica (69°S) on board the MV *SA Agulhas*. Sampling included both
182 (Antarctic) coastal and open ocean waters during this cruise.

184 During the BoBBLe and SOE9 cruises, surface water samples were obtained manually from
185 the upper 30-70 cm of the sea surface using a metal bucket deployed over the side of the ship
186 near the stern. Additional depth profile samples were obtained using a CTD (911 plus, Sea-
187 Bird Electronics, USA) rosette equipped with 12 Niskin bottles. During the SOE9 cruise,
188 depth profiles were taken at 17 CTD stations, and additional surface samples were taken (by
189 bucket) at least twice a day along the entire cruise track (except when the ship was stationary
190 for CTD stations). Sampling included two time-series, one at ~40°S, and one in coastal
191 Antarctic waters at ~68°S (around the Polar Front), during which samples were collected at 4
192 or 6 hour intervals for up to 72 hours. During the SK333 cruise, samples were only collected
193 using a CTD rosette. Sample dates, times and locations for all cruises are given in the online
194 dataset available from the British Oceanographic Data Centre (http://doi.org/czhx). In this
195 manuscript, both shallow CTD samples (depth ≤ 10 m) and 'bucket' samples will be
196 considered to be comparable, and representative of the ocean surface. This follows the
197 approach taken in previous examinations of sea surface iodide concentrations (Chance et al.
198 2014). Note only surface samples are considered in this manuscript, although selected depth
199 profiles are presented in the Supplementary information to aid interpretation of surface
200 concentrations.

202 Immediately following collection, samples were filtered (Whatman GF/F) under gentle
203 vacuum, and transferred to 50 mL polypropylene screw cap tubes. Duplicate aliquots were
204 prepared for each sample. Aliquots were either stored at 4° C for on-board iodide
205 determination within 24 hours, or frozen at -20° C for transport back to our laboratories for
206 analysis. Analysis of frozen samples took place within 18 months of collection. Inorganic
207 iodine speciation is preserved in frozen samples (≤-16° C) for at least one year (Campos
208 1997). To avoid possible contamination, sample bottles for the iodine samples were kept
209 strictly separated from the dissolved oxygen reagents containing iodine.

211 *Iodide and iodate analysis*
212 Iodide was determined by cathodic stripping square wave voltammetry (Campos 1997;
213 Luther, Swartz, and Ullman 1988) using a µAutolab III potentiostat connected to a 665VA
214 stand (Metrohm) with a hanging mercury drop electrode, an Ag/AgCl reference electrode and
215 a carbon or platinum auxiliary electrode. 12 (or 15) mL of the sample was introduced to a
216 glass cell and 90 (or 112) µL of Triton X-100 (0.2%) was added. The sample was purged
217 with N_2 (oxygen free grade) for 5 minutes before each measurement. The deposition potential
218 was set at 0 V and deposition times were typically 60 s; scans ranged from 0 to -0.7 V, with a
219 step of 2 mV, a 75 Hz frequency and a 0.02 V wave amplitude. Each scan was repeated 5-6
220 times, with scan repeatability equal or better than 5%. Calibration was by 2 or 3 standard
221 additions of a KI solution (~10^5 or 10^6 M). Precision was estimated by repeat analysis (n = 6)
222 of selected seawater samples over period of ten days and was found to be lower than 7%
223 relative standard deviation.

225 Iodate was measured using a spectrophotometer (UV-1800, Shimadzu; 4 decimal places)
226 after reduction to iodonium (I_3) (Jickells, Boyd, and Knap 1988; Truesdale and Spencer
227 1974). 2.3 mL of the sample was introduced in the 1 cm UV quartz cell, 50uL of sulfamic
228 acid (1.5 M) was added, and the first absorbance value was obtained after 1 minute. Then 150
229 µL of KI (0.6 M) was added and the second absorbance read after 2.5 minutes. Iodate

concentrations were calculated from the difference between the two absorbances. Calibration was performed daily using a series of KIO_3 standard solutions. Samples were measured at least in triplicate with repeatability better than 5%; reported values are means. Reported errors are calculated by propagation of the standard deviation on the repeated measurements, the errors on the fit of the calibration and error on the volumes pipetted. Note that strictly, this method measures all inorganic iodine in oxidation states from 0 to +5, but as this fraction is dominated by iodate it is taken as a measure of iodate.

Supporting measurements

Samples from CTD stations use the temperature, salinity and depth data directly obtained from the CTD. Precision of these measurements was as follows: temperature: ± 0.001 °C; conductivity: ± 0.0001 S m^{-1}; depth: ± 0.005% of the full scale. CTD salinity was calibrated using a high-precision salinometer (Guildline AUTOSAL). Temperature and salinity of manually collected 'bucket' samples were determined using an outboard thermometer, and the salinometer respectively.

Samples for nitrate (NO_3) analysis were collected in 250 mL narrow mouth polypropylene amber bottles (Nalgene). Each bottle was rinsed twice with the sample water prior to collection. Analysis was performed onboard as soon as possible after sample collection, using an SKALAR SAN+ segmented continuous flow autoanalyzer. Precision and accuracy of NO_3 measurements were ±0.06 and ±0.07 μM, respectively.

Ocean Modelling

The ocean iodine cycling model described in Wadley et al. (Wadley et al. 2020) was used to evaluate which physical and biogeochemical processes drive the observed trends in iodide concentration in the Indian Ocean and Indian sector of the Southern Ocean. The model comprises a biogeochemical model of iodine cycling embedded in a three-dimensional global ocean circulation framework, and has been calibrated using the data from a recently available extended global sea surface iodide compilation (Chance, Tinel, Sherwen, Baker, Bell, Brindle, Campos, Croot, Ducklow, He, Hopkins, et al. 2019) which includes the current data set, plus additional depth resolved iodide measurements (see (Wadley et al. 2020) for details). In the model, iodide production is driven by primary production, and iodide loss (by oxidation) is linked to biological nitrification. A spatially variable I:C ratio is used to allow the model to better capture the observed iodide concentrations.

Results and Discussion

Overview – Global scale trends

In total, 127 new sea surface iodide observations and 130 sea surface iodate observations are reported here for the three cruises, including two time series. Measurements were made at 98 different sampling locations, spanning latitudes from ~12°N to ~70°S. This is a substantial increase in data coverage for the Indian Ocean and the Indian sector of the Southern Ocean region, which was previously particularly lacking in observations of sea surface iodine speciation (Chance et al. 2014). As noted in the introduction, only two sea surface iodide observations for the Indian Ocean were included in Chance et al., 2014, and both were from the Arabian Sea (see Figure 1).

[Figure 2]

[Figure 3]

281   The highest iodide concentrations were observed in and approaching the tropics, while lower
282   concentrations were observed at high latitudes (Figure 2). This latitudinal trend in sea surface
283   iodide concentration broadly follows those observed in other ocean basins (Figure 3). In
284   addition, a 'dip' in sea surface iodide concentrations is seen around the equator and elevated
285   concentrations are seen in coastal polar waters, as observed elsewhere (Figures 2 & 3)
286   (Chance et al. 2014; Chance et al. 2010). While these global scale trends are well
287   documented in the Atlantic and Pacific basins e.g.(Bluhm et al. 2011; Campos, Sanders, and
288   Jickells 1999; Truesdale, Bale, and Woodward 2000; Tsunogai and Henmi 1971), to the best
289   of our knowledge this is the first time they have been confirmed in the Indian Ocean and the
290   Indian section of the Southern Ocean.

291

292   *[Figure 4]*

293

294   Considering the entire data set (n=127), sea surface iodide concentrations ranged from 20 to
295   1241 nM, with a median of 61 nM (Figure 4). The very large range in the data is primarily
296   due to the presence of two very high outliers in the Bay of Bengal, which are discussed later
297   (Section 3.3). When these outliers are excluded, the upper limit of the data is reduced to 250
298   nM, bringing the range within the global range of marine iodide concentrations previously
299   reported (Chance et al. 2014). The large range in the overall data set can mainly be ascribed
300   to the large span of latitudes covered. The median value is somewhat lower than the global
301   median value (77 nM; (Chance et al. 2014), reflecting the bias towards high latitude/low
302   iodide samples in our data set.

303

304   *[Figure 5]*

305

306   Sea surface iodate concentrations ranged from 51 to 495 nM, with a median of 294 nM.
307   Iodate concentrations broadly showed the opposite pattern to iodide concentrations, with
308   highest median values in the Southern Ocean (median of 323 nM), intermediate values in the
309   subtropical Indian Ocean (median of 294 nM) and lowest values in the tropical Indian Ocean
310   (median 196 nM). However, there was only a very weak, inverse linear relationship between
311   sea surface iodide and iodate concentrations ($R^2 = 0.16$, $p = 3$ x 10^{-6}; Figure 5). Total iodine
312   concentrations in seawater are typically ~450 nM ((Chance et al. 2014) and references
313   therein), with the budget dominated by iodide and iodate. Here we find the sum of iodide and
314   iodate was less than this at most sampling locations (Figure 5), with a median value of 380
315   nM (range 88 to 560 nM). Although somewhat unusual, comparable low total inorganic
316   iodine concentrations have been reported elsewhere (e.g. North Sea (Hou et al. 2007), South
317   East China Sea (Wong and Zhang 2003)). Depleted total inorganic iodine may be due to the
318   uptake of iodine to the particulate phase in the surface ocean, or to the presence of a
319   significant dissolved organic iodine reservoir. Although it could imply substantial loss of
320   iodine from the surface ocean to the atmosphere, current knowledge suggests the magnitude
321   of such fluxes (e.g. (Carpenter et al. 2013)) is too small to have such a large impact on the sea
322   surface concentrations. No clear relationships were evident between total inorganic iodine
323   and either latitude or nitrate concentration.

324

325   Our sampling area spanned a wide range of different water masses and biogeochemical
326   conditions (Figure 2). Low temperature waters at high latitudes were characterised by high
327   nitrate and low iodide concentrations, while further north in the subtropical gyre, nitrate
328   concentrations were very low and iodide concentrations rose in step with decreasing latitude
329   and increasing SST (Figure 2). North of the equator, SST becomes a poor predictor of iodide

330 concentration. To explore our data set further, we consider iodine speciation separately in
331 each of three different hydrographic regimes (tropical, mid-latitudes and polar).
332
333 ***South Indian subtropical gyre (~23-42 °S)***
334 Samples were collected from the southern Indian Ocean (~23-42 °S) during the SOE9 cruise.
335 The samples form an approximate latitudinal transect along 57°E, encompassing the Indian
336 South subtropical gyre and the subtropical convergence zone. All are open ocean. North of
337 this region, the Southern Equatorial Current (SEC; not sampled in this work) has been noted
338 as a clear biogeochemical front, separating subtropical gyre waters from the lower oxygen
339 northern Indian Ocean (Grand et al. 2015). The subtropical gyre waters are characterised by
340 very low nitrate concentrations and relatively high salinity (Figure 2), with SST rising from
341 ~15°C in the south to ~29°C in the north.
342
343 Between these latitudes, iodide concentrations ranged from 35 to 235 nM and increased in an
344 approximately linear manner with decreasing latitude. In this region, iodide is strongly
345 correlated with both latitude ($R^2 = 0.86$, p = 3 x 10^{20}) and SST ($R^2_{adj} = 0.89$, p = 2 x 10^{22}). These
346 are stronger correlations than the global relationships reported in Chance et al., 2014, and
347 also have steeper gradients (Table 1). Using the extended dataset of global sea surface iodide
348 observations (Chance et al., 2019), sea surface iodide gradients in each of the ocean basins
349 were compared. Considering each of the major ocean gyres individually reveals that the
350 latitudinal dependency of iodide is greater in the Indian Ocean than in the north Atlantic,
351 north Pacific, south Pacific (excluding observations from the Peruvian upwelling, which do
352 not conform to a linear latitudinal trend) or south Atlantic (Figure 3; Supp Info Table 1). This
353 trend is driven by concentrations at the northern limit of our Indian Ocean observations
354 (~25°S) being approximately double those at comparable latitudes in the other ocean basins,
355 rather than a difference between concentrations at the poleward limit (Figure 3).
356
357 The same trend is also evident when the relationships between iodide and SST are
358 considered. Although SST is not thought to directly impact iodine cycling itself, this
359 relationship is important as it is widely used to predict sea surface iodide concentration fields
360 for use in atmospheric models (e.g. (Sarwar et al. 2016)). The observed iodide vs. SST
361 gradient is steeper in the Indian Ocean than other basins (Supp Info Table 1), implying the
362 differences between basins cannot entirely be accounted for by differences in SST gradients.
363 In any case, examination of climatological data (World Ocean Atlas, see Chance et al., 2014
364 for details) for the locations and months of iodide observations does not demonstrate any
365 clear differences in SST, nitrate or mixed layer depth (MLD; defined using potential
366 temperature) between ocean basins that might account for the difference in iodide gradient.
367 This is explored further in Section 4.2. As a result, the stronger latitudinal dependency of
368 iodide in the Indian Ocean that we observe here is not replicated in sea surface iodide values
369 predicted using commonly employed parametrisations based on sea surface temperature
370 (Chance et al. 2014; MacDonald et al. 2014). This is likely to introduce uncertainties specific
371 to the Indian Ocean when using such parameterisations, for example in model calculations of
372 iodine emissions from the sea surface.
373
374 The observational data is too limited to properly evaluate whether the pattern is the result of
375 seasonal biases in sampling; all subtropical Indian Ocean observations were made during the
376 southern hemisphere summer (January and February), while the modal months for
377 observations in other basins were November (North Atlantic and South Pacific), October
378 (South Atlantic) and March (North Pacific), see table S1. In the South Pacific, 90% of
379 observations were made in January, i.e. in the same season as the Indian Ocean data. Despite

380 this, they have a lower latitudinal gradient (m = 2.8 compared to 9.5; table S1), hinting that
381 the difference between basins is not due to seasonal variation and/or sampling biases and may
382 instead be due to differences in iodine cycling.
383
384 With the exception of one higher value of 1.45 μM, observed sea surface nitrate
385 concentrations in this region were generally low, with 86% of data points being below 0.5
386 μM. No relationship between nitrate and iodide was apparent (R^2 = 0.0004; Table 1),
387 implying sea surface nitrate concentrations are a poor predictor of sea surface iodide in this
388 hydrographic region. This likely reflects the fact nitrate concentrations were all very low,
389 while substantial gradients in iodide concentrations were present. Campos et al. (Campos,
390 Sanders, and Jickells 1999) have previously reported significant relationships between iodide
391 and nitrate in the subtropical Atlantic, but as these were based on measurements from the
392 upper 100 m of the water column rather than just the surface, and encompassed a range of
393 nitrate concentrations, they are not directly comparable.
394
395
396   *[Table 1]*
397
398
399 ***Southern Ocean domain (~42˚S - 68˚S)***
400 At the subtropical front around 42˚ S, a decrease in salinity is accompanied by a sharp
401 increase in nitrate concentration (Figure 2). This front marks the transition from the Indian
402 Ocean to the Southern Ocean (Orsi, Whitworth, and Nowlin 1995). The colder, nutrient rich
403 waters south of the subtropical front have much lower iodide content, with a median
404 concentration of 43 nM and range of 20 to 104 nM (Figure 4). Relationships between iodide
405 concentrations and latitude or SST are much weaker than those observed further north (Table
406 1). This may be due to disruption by strong, but variable, vertical mixing events, which are
407 characteristic of the Southern Ocean. No significant relationship between sea surface iodide
408 and nitrate was observed in the Southern Ocean samples (Table 1). Negative correlations
409 between iodide and nitrate have previously been reported for the upper 500 m of the water
410 column in the Atlantic sector of the Southern Ocean, including the Weddell Sea (Campos,
411 Sanders, and Jickells 1999), but were not replicated in a later study in the same area (Bluhm
412 et al. 2011). At an Antarctic coastal site, only weak negative correlations between iodide and
413 nitrate concentrations were observed (Chance et al. 2010).
414
415 The Southern Ocean samples may be further subdivided into coastal (i.e. near the Antarctic
416 continent) and open ocean samples. The former category was defined as samples falling
417 within the Austral Polar biogeochemical province (Longhurst 1998), while the latter category
418 included samples from both the Antarctic and Sub-Antarctic provinces, and spanned the Polar
419 Front. The range and distribution of concentrations seen in the coastal and open ocean subsets
420 are very similar (Figure 4), despite the coastal samples spanning a much narrower latitudinal
421 range (69 - 64° S, compared to 63 - 43° S). In the open ocean sub-set, iodide concentrations
422 generally decrease moving south (R^2 = 0.16; p = 0.04), while in the coastal samples at the
423 most southerly extreme of the data set, this relationship breaks down (R^2 = 0.02; Figure 2). A
424 similar pattern is also reported in the global compilation of Chance et al. (2014), where
425 Southern Ocean and Antarctic samples were predominantly from the Atlantic sector and the
426 western Antarctic Peninsula. The range of concentrations observed in the Antarctic coastal
427 samples (20 to 95 nM) is within that observed previously in coastal Antarctic waters during
428 the austral summer (Chance et al. 2010). The magnitude of this variability is greater than can

be accounted for by normalizing the iodide concentrations to salinity variations (e.g. due to
ice melt water).

Northern Indian Ocean including southern Bay of Bengal (~4° S - 11° N)

Samples were collected from tropical waters in the northern Indian Ocean during the
BoBBLe (Bay of Bengal) and SK333 (Arabian Sea) cruises. The latitudinal range of this
sample sub-set was ~4° S to ~11° N, and all were considered to be open ocean. These
sampling locations were within the Indian Monsoon Gyre biogeochemical province, and
shared high sea-surface temperatures, variable salinity and typically low nitrate
concentrations. This sample sub-set showed the highest, and most variable iodide
concentrations (range 63 to 1241 nM, median 165 nM; Figure 4). This was primarily due to
the occurrence of two extremely high iodide concentrations (>900 nM) in the Bay of Bengal;
excluding these values, the range in tropical open ocean iodide was still the largest of the
three hydrographic regions surveyed, with a maximum of 250 nM being observed in the Bay
of Bengal (Figure 4). Such concentrations are comparable to measurements made at similar
latitudes elsewhere (Figure 3).

All but one of the samples collected around the equator (~5°S to ~3°N) during the SK333
cruise had iodide concentrations in the range ~80 to 120 nM. The exception to this was at
67°E, 0°N (CTD2), where iodide concentrations reached ~200 nM. As iodide concentrations
were typically lower than in tropical waters further north and south (Figure 2), there was a
positive rather than negative correlation between iodide and absolute latitude in this sample
set (Table 1). A similar dip at very low latitudes is also seen in the Atlantic and Pacific
(Figure 3; Chance et al., 2014). This feature is replicated in our model and is thought to be
due to equatorial upwelling (see Section 4).

As already noted, exceptionally high sea surface iodide concentrations of 1241 and 949 nM
were observed at two stations in the Bay of Bengal (UWI BS3 & UWI BS8). Very high near-
surface iodide concentrations were also observed at Station AR nearby (2039, 1546 & 479
nM at 10, 25 & 50 m respectively; see Figure S1 in Supplementary Information). We believe
these concentrations are real, and not the result of contamination or analytical error because:
(i) repeat analyses gave the same results, (ii) very high concentration samples were also
analysed by ion chromatography, a completely independent method, and this yielded
concentrations within 10% of those obtained by voltammetry (1277 and 960 nM for samples
BS3 and BS8 respectively, and 1693 nM for Station AR at 25 m depth), (iii) results for
station AR show oceanographic consistency (see Figure S1), (iv) no likely sources of iodine
contamination were present during sampling. It is possible that the high, very localised,
iodide concentrations could arise from the break-down of an iodine rich substrate, for
instance a mass of brown macroalgae such as Laminaria digitata. However, nothing unusual
of this nature was observed during sampling. These very high iodide levels result in total
(dissolved) inorganic iodine concentrations several times higher than the near universally
observed value of ~500 nM (Chance et al. 2014). They cannot be accounted for by the
reduction of iodate, and instead imply an exogenous source of iodide-iodine.

Samples with elevated iodide exhibited relatively low surface salinity (Figure S1, Supp Info),
possibly indicating an association with freshwater inputs. The Bay of Bengal is characterized
by very heterogenous salinity - low salinity is caused by monsoon rainfall and high riverine
inputs to the north, while high salinity water arrives from the Arabian Sea via the intense
Southwest Monsoon Current (SMC). The BoBBLe cruise took place during the Asian
summer monsoon season, during which the region experiences high rainfall. However,

479 atmospheric wet deposition is thought unlikely to be the source of elevated iodide because
480 meteoric water has a lower iodine content than seawater (20-124 nM (Sadasivan and Anand
481 1979); 4.7-26.2 nM; (Gilfedder, Petri, and Biester 2007)). Furthermore, observations of
482 elevated sea surface iodide did not correspond to rainfall events encountered during the
483 BoBBLe cruise itself. Similarly, riverine inputs are unlikely to be the iodide source, as total
484 iodine concentrations in rivers, including the Ganges, are lower than or comparable to those
485 in seawater ($\leq$ 20 ug/L, $\sim$ 157 nM; (Moran, Oktay, and Santschi 2002; Ghose, Das, and Saha
486 2003)), and the area surveyed was away from major outflows. While freshwater inputs are
487 thus not thought to be the source of the excess iodide, stratification caused by rainwater
488 dilution of surface layers could perhaps contribute to the persistence of high iodide
489 concentrations at the ocean surface.
490
491 In addition to the SMC, the second main oceanographic feature in the BoBBLe study area is a
492 wind driven upwelling feature called the Sri Lanka Dome (SLD), which manifests as a large
493 cyclonic gyre in the south western part of the BoB to the east of Sri Lanka. The SLD is
494 identified as an area of negative mean sea level anomaly and a relatively shallow
495 thermocline. Both the SLD and the SMC were well developed and distinct during the study
496 period (Vinayachandran et al. 2018). Extreme iodide values were observed at stations north
497 (AR, BS3) and east (BS8) of the SLD, but not in the stations that were inside the SLD
498 (Figure S2, Supp Info) (Vinayachandran et al. 2018). High iodide station AR exhibited high
499 seawater pCO_2 (467–554 atm), low surface pH and low alkalinity, indicative of upwelled
500 waters that are presumed to be associated with the SMC (Vinayachandran et al. 2018).
501 Station BS3 was close in space and time, while station BS8 was also influenced by the SMC
502 (Vinayachandran et al. 2018). We therefore speculate that the high iodide observed is in some
503 way related to the SMC. However, the high salinity core of the SMC (i.e. Arabian Sea water),
504 which was evident at depths of $\sim$25-150 m at stations east of the SLD, was not itself
505 associated with elevated iodide (Figure S1, Supp Info). This suggests the excess iodide was
506 not in the main water mass carried by the SMC, and did not originate from the Arabian Sea.
507
508 Comparable high iodide concentrations have previously been observed in low oxygen sub-
509 surface waters in the north western part of the Arabian Sea (Farrenkopf and Luther 2002);
510 these were attributed to advection from shelf sediments. More recently, plumes of very high
511 iodide sub-surface concentrations ($\sim$1000 nM) have also been reported in sub-oxic waters in
512 the Eastern Tropical South Pacific (ETSP) (Cutter et al. 2018) and the Eastern Tropical North
513 Pacific (ETNP) (Moriyasu et al. 2020). In the ETSP, the plume followed an isopycnal and
514 was associated with corresponding features in Fe(II) and nitrite, so was again thought to be
515 due to a shelf sediment iodide source (Cutter et al. 2018). Elevated concentrations persisted
516 more than 1000 km from the shelf break due to the relatively long iodide lifetime in seawater
517 with respect to oxidation. Trace metal concentrations were not measured during the BoBBLe
518 cruise, but sub-surface waters in the region have previously been reported to contain
519 additional dissolved Fe from sedimentary inputs (Grand et al. 2015), suggesting it is plausible
520 that stations on the edge of the SLD could be influenced by sedimentary interactions. Waters
521 over the western Indian shelf experience severe hypoxia (Naqvi et al. 2000), and so could be
522 subject to significant sedimentary iodide inputs as implicated in other low oxygen regions
523 (Cutter et al. 2018; Farrenkopf and Luther 2002). During the Southwest Monsoon, the West
524 Indian Coastal Current (WICC) flows south along the west coast of India, and these waters
525 are advected along the path of the SMC into the BoB. We speculate that such waters have
526 potential to contain 'excess' iodide levels as a result of sedimentary inputs, and that it is the
527 remnants of these water masses that we may have sampled.
528

529 We believe this is the third reported observation of very elevated (>500 nM) iodide
530 concentrations at the surface of the open ocean. The dataset reported by Cutter et al. (2018)
531 contains two surface samples with iodide concentrations of 594 and 960 nM immediately off
532 the coast of Peru, while transects in (Moriyasu et al. 2020), show patches of high iodide
533 outcropping at the surface. An extreme surface iodide concentration of ~700 nM has also
534 been reported for the brackish waters of the Skaggerrak (Truesdale, Danielssen, and Waite
535 2003), a shallow strait that is subject to hypoxia (Johannessen and Dahl 1996). The paucity of
536 previous observations suggests it is a rare phenomenon, but it may nonetheless be of local
537 significance. Atmospheric ozone deposition and iodine emission fluxes will proportionally
538 increase where surface iodide concentrations are high. An increase in iodide from 150 to
539 2050 nM (x 13.7) leads to a 5-6 fold increase in total iodine emissions, for a typical ambient
540 ozone concentration of 25 ppb and a wind speed of 7 m s^{-1} (Figure S3, Supp Info). This
541 comprises a 4.5-fold increase in HOI emissions, which dominates the flux, and a 30-fold
542 increase in I$_2$ emissions, which increase from 5.5% of the total flux at 150 nM iodide to 28%
543 at 2050 nM iodide. It is assumed that the regional atmospheric impact of such 'hot-spots' will
544 be low, as they will only represent a small proportion of the relevant footprint area. However,
545 the atmospheric impacts of such areas may become significant if either very localised
546 processes are being considered, or their extent and/or frequency of occurrence increases. As
547 areas of low oxygen waters in contact with shelf sediments become more extensive (Naqvi et
548 al. 2000), the possibility that this could impact on surface iodide concentrations in coastal
549 regions may need to be considered. Understanding the potential impact of low oxygen
550 conditions and sedimentary inputs on surface iodide concentrations, and hence local
551 atmospheric chemistry, requires both the sedimentary fluxes and the lifetime of iodide in
552 oxygenated seawater to be better constrained. The atmospheric boundary layer above the
553 northern Indian Ocean has high iodine oxide (IO) levels, with inputs dominated by the
554 inorganic iodine flux from the ozone-iodide reaction (>90%), as a result of "ozone-related"
555 pollution outflow (Prados-Roman et al. 2015). Hence atmospheric chemistry in the region
556 may be particularly sensitive to changes in the surface iodide budget.
557
558 **Exploring controls on the sea surface iodide distribution in the Indian Ocean using an**
559 **ocean iodine cycling model**
560
561 The trends in sea surface iodide concentrations observed across the south Indian subtropical
562 gyre and Indian sector of the Southern Ocean are well replicated by the iodine cycling model
563 of Wadley et al. (Wadley et al. 2020) (Figure 6a). In the northern Indian Ocean agreement
564 between model and observations is poorer, but modelled concentrations fall within the range
565 of the observations in the area. Furthermore, the model predicts unusually high iodide
566 concentrations in the BoB, where extremely high iodide concentrations were observed. Note
567 the model does not currently include sedimentary processes, so this suggests that additional
568 physical and biogeochemical processes may also contribute to elevated iodide levels in the
569 BoB. Given the generally good agreement between observed and modelled iodide
570 concentrations, we explored the controls on the iodide distribution in the study area by
571 examining the physical and biogeochemical drivers of iodine cycling within the model.
572
573 *The influence of physical and biogeochemical processes on the iodide distribution*
574 The sea surface iodide distribution is thought to result from the interplay of biological
575 formation and loss processes, and physical mixing and transport (Chance et al., 2014), and
576 these processes are represented in the iodine cycling model (Wadley et al. 2020). Biological
577 productivity drives iodide formation in the model, but direct associations between the spatial
578 distribution of productivity and iodide (either observed or simulated) are not seen in the

579   Indian Ocean basin (Figure 6a, b). Most notably, the strong peak in productivity centred on
580   40°S (Figure 6b) has no corresponding peak in either observed or simulated iodide
581   concentrations. This indicates that other processes are also important in determining the
582   iodide distribution. Imposing a constant level of productivity (set at the annual mean for each
583   grid point) throughout the year had very little effect on modelled iodide concentrations,
584   (Figure 6c), suggesting that the relationship between the seasonal cycle of iodide production
585   and physical factors (e.g. MLD, see below) does not have a significant effect on iodide
586   concentrations. Halving the productivity in the model reduces simulated iodide
587   concentrations by around a half south of 40°S (where iodide is very low, and iodate high), but
588   only by around a quarter north of 40°S, and has almost no effect in the northern Indian Ocean
589   where modelled iodide is highest (and thus modelled iodate lowest, at ≤ 300 nM). This may
590   indicate that lower iodate concentrations to the north limit iodide production. The amount of
591   iodide produced per unit primary productivity is specified in a spatially variable I:C ratio
592   (Figure 6e; (Wadley et al. 2020). Halving this ratio is equivalent to halving primary
593   production, and has identical consequences (Figure 6f).
594
595   Iodide produced by primary productivity is distributed throughout the mixed layer, and
596   surface concentrations are therefore dependent on the MLD. Summer MLD minima are
597   similar throughout the section, with typical values of a few tens of metres, whereas late
598   winter MLD maxima increase with latitude (Figure 6j).
599   Deepening of the MLD decreases iodide concentrations throughout the mixed layer as a
600   result of dilution, while shoaling of the MLD decreases the total amount of iodine present
601   integrated over the mixed layer, but does not change the concentration at any given depth
602   within it. Removing the seasonal cycle of MLD in the model (by replacing with the annual
603   mean MLD for each grid point) increases surface iodide concentrations, particularly at lower
604   latitudes (Figure 6k), indicating that the removal of iodide through MLD shoaling is
605   important. Removing both seasonal and spatial variation in the MLD by setting it to a
606   uniform 56 m results in substantial increases in surface iodide concentrations at higher
607   latitudes (Figure 6l), due to elimination of both dilution and shoaling effects. In contrast,
608   doubling the MLD decreases iodide concentrations, with the greatest effect seen where iodide
609   concentrations are highest (Figure 6m). Interestingly, this brings modelled and observed
610   iodide concentrations into good agreement around the equator. Inspection of SK333 CTD
611   data indicates that at the time of sampling, actual MLDs in this region (between 50 to 100 m)
612   were deeper than the climatological values used in the model (less than 40 m; Figure 6j),
613   which may indicate that short term variations in MLD, for example due to weather events,
614   affected iodide concentrations. In the model, the release of iodide from phytoplankton occurs
615   60 days after the uptake of carbon, and the interplay of this lag period with the MLD cycle
616   could influence iodide concentrations. However, changing the duration of the lag to 0 and
617   120 days in the model has only a small impact on the iodide, and only at high latitudes
618   (Figures 6g and 6h).
619
620   The seasonal MLD cycle imposes an annual timescale on the removal of iodide from the
621   mixed layer where the seasonal cycle has a large amplitude, but vertical and horizontal
622   advection also exchange water between the surface layer and ocean interior. Turning off the
623   circulation in the model, so that vertical mixing is the only physical mechanism for iodide
624   removal from the mixed layer also results in increased mixed layer iodide concentrations at
625   almost all locations (Figure 6n), In addition to removal by MLD shoaling, the model also
626   allows for the removal of mixed layer iodide by oxidation to iodate, via a pathway linked to
627   nitrification ((Hughes et al. 2020; Wadley et al. 2020)). Eliminating this pathway has little
628   impact on modelled iodide concentrations at high latitudes, but results in a significant

629 increase in concentrations north of 40°S (Figure 6i). This is because the iodide oxidation
630 timescale in the model is multi-annual, and hence its impact is modulated by the lifetime of
631 iodide in the mixed layer with reference to vertical mixing. At high latitudes, large seasonal
632 changes in the MLD result in low sensitivity to oxidation, whereas at lower latitudes there is
633 less annual mixed layer exchange, resulting in a longer iodide residence time, and hence
634 oxidation is a more important process for mixed layer iodide removal.

636 The net surface fresh water flux resulting from precipitation and evaporation acts to
637 respectively dilute or concentrate iodide in the mixed layer (Figure 6o). Setting the P-E flux
638 to zero has a small impact on iodide, decreasing concentrations in the subtropical gyres where
639 evaporation is strong. Thus at these latitudes evaporation results in a modest increase in
640 iodide concentrations.

642 The model sensitivity tests described above confirm that sea surface iodide concentrations in
643 the Indian and Southern Oceans are determined by a combination of factors which interact
644 non-linearly. The dominant processes that determine iodide concentrations are the rate of
645 iodide production, which is a function of productivity and the I:C ratio, and the MLD and its
646 seasonal cycle, which acts to dilute and remove iodide from the surface layer. Loss by
647 oxidation has the greatest impact at lower latitudes where physical removal mechanisms are
648 weakest. As the climate changes over coming decades, changes in any of these factors are
649 likely to result in changes in sea surface iodide concentrations. For example, the 100 to 300
650 m depth layer in the Indian Ocean has significantly warmed since 2003 as a result of heat
651 distribution from the Pacific (Nieves et al., 2015) and this is likely to reduce stratification,
652 and enhance vertical mixing, with an accompanying reduction in mixed layer iodide
653 concentrations. Conversely, changes in nutrient inputs to the Indian Ocean and declining
654 oxygen levels will act to reduce iodide oxidation, due to its association with nitrification
655 (Hughes et al. 2020), and hence may act to increase iodide concentrations. Any changes in
656 productivity, and/or shifts to different phytoplankton types with different I:C ratios, will also
657 potentially alter the rate of iodide production, although this has been found to predominantly
658 impact on iodide concentrations at higher latitudes (Wadley et al., *Manuscript In*
659 *Preparation*).

662 *[Figure 6]*

664 ***Difference in latitudinal iodide gradients between the subtropical Indian and Atlantic***
665 ***Oceans***
666 As described earlier, observed sea-surface iodide concentrations have a steeper latitudinal
667 gradient (and related SST dependency) in the subtropical Indian Ocean than reported for
668 other ocean basins (Supplementary Information, Table S1), and this may limit the accuracy of
669 global scale parameterisations relating iodide to SST. Although less pronounced, this feature
670 is replicated in the model output (see table S1), and therefore a series of sensitivity tests have
671 been conducted to investigate which processes may be responsible for the apparent
672 differences in the latitudinal iodide gradient between ocean basins. Specifically, the model
673 was run with each of the iodide forcing processes in the Indian Ocean and Indian sector of the
674 Southern Ocean replaced by those from the Atlantic. Figure 7 shows the forcing fields used
675 for the two ocean basins, and the modelled iodide concentrations generated using these fields.
676 The gradient of iodide against latitude is significantly increased between 30°S and 20°S when
677 the Indian Ocean and Indian sector of the Southern Ocean productivity fields are replaced
678 with values for the same latitudes in the Atlantic. This is driven by a smaller decrease in

679 productivity with decreasing latitude in the Indian Ocean than the Atlantic. Thus productivity
680 differences act to decrease, rather than increase the iodide gradient. Removal of iodide from
681 the mixed layer by oxidation occurs as a function of nitrification (Wadley et al. 2020), which
682 is parameterised using the proportion of nitrate regenerated in the mixed layer (see Yool et
683 al., 2007). Differences between this ratio in the subtropical regions of the Indian and Atlantic
684 oceans are small (Figure 7d), and have negligible impact on the modelled iodide in the Indian
685 Ocean (Figure 7e). At lower latitudes MLDs are similar in the two basins, but between ~35
686 and 45°S, MLDs are significantly deeper in the Atlantic due to the greater northward extent of
687 polar waters (Figure 7f). Since a deeper MLD dilutes iodide, modelled iodide concentrations
688 are lower between 45°S and 35°S with Atlantic MLDs imposed in the Indian basin (Figure
689 7g), and this increases the latitudinal gradient of iodide, contrary to the observed difference in
690 gradients between the basins. Precipitation and evaporation act to dilute/concentrate iodide in
691 the mixed layer, so changes in the net fresh water flux with latitude could influence the
692 latitudinal iodide gradient. The model was run with the Atlantic surface fresh water flux
693 imposed in the Indian Basin (Figure 7h). This was found to have a negligible effect on iodide
694 (Figure 7i). Finally, the I:C ratio in the model determines the amount of iodide produced per
695 unit carbon of primary production. This ratio is found to be greater (more iodide produced
696 per unit carbon) in the Indian than Atlantic Ocean to allow the model to fit the observed
697 iodide in each basin (Figure 7j). The I:C ratio in the Indian Ocean was replaced by that for
698 the Atlantic Ocean in the model (Figure 7k). This results in decreased iodide production, and
699 iodide concentrations, but the latitudinal gradient of iodide shows little overall change
700 between 41°S and 23°S. It should be noted that the model does underestimate the iodide
701 gradient in the Indian Ocean (See Table S1), and refinement of the spatial variation of the I:C
702 ratio in the model to improve the model fit to observations is likely to show that it is the I:C
703 ratio which is responsible for the greater observed latitudinal gradient of iodide in the model.
704
705 In summary, basin scale differences in the above four forcing fields investigated here
706 (productivity, nitrification, MLD and P-E) do not appear to explain the difference in
707 latitudinal iodide gradient between the subtropical Indian and southern Atlantic oceans. In
708 fact, differences in productivity and MLD between the two basins would appear to have the
709 opposite effect, with Atlantic forcing fields resulting in a steeper gradient than Indian Ocean
710 forcing fields. The above analysis implies that the difference in sea-surface iodide
711 concentration gradient between the Indian Ocean and the other ocean basins is not the result
712 of geographical or seasonal differences in either physical mixing and/or ocean circulation, or
713 primary production, as these features are accounted for by the model. Instead we suggest the
714 difference may be the result of different phytoplankton types, with differing I:C iodide
715 production ratios, in the two basins. A spatially variable I:C ratio is used in the model to
716 allow the model to fit the global observations (Wadley et al. 2020), and across all latitudes
717 this is higher for the Indian Ocean/Indian sector of the Southern Ocean than the Atlantic. The
718 need for this I:C ratio adjustment implies that the difference might instead arise from
719 differences in microbiological community composition, and/or the expression of metabolic
720 processes by such organisms. *Synechococcus* dominates in the subtropical Indian Ocean,
721 whereas Nanoeucaryotes and *Prochlorococcus* dominate in the subtropical Atlantic (Alvain
722 et al., 2008). Recent work by our group indicates that the I:C ratio associated with iodide
723 production varies between phytoplankton types, with *Synechococcus* having a higher I:C
724 ratio than Nanoeucaryotes and *Prochlorococcus* types (Wadley et al., *Manuscript in*
725 *Preparation*). Hence the higher relative abundance of *Synechococcus* in the subtropical
726 Indian Ocean might account for the higher iodide concentrations observed at low latitudes,
727 and the resulting steeper sea-surface iodide gradient. This also indicates that any change in

728　microbiological community composition associated with climate change could significantly
729　impact ocean iodide concentrations.
730
731　*[Figure 7]*
732
733
734　**Concluding remarks**
735　This study has contributed 127 new sea surface iodide observations to the available
736　measurements, which represents a substantial (>10%) increase in the number of available
737　measurements (925 individual observations were included in Chance et al., 2014). The
738　observations span nearly 80 degrees latitude in the Indian Ocean and Indian sector of the
739　Southern Ocean, a region where very few (n=2) surface observations were previously
740　available. Increased observations will facilitate better predictions of sea surface iodide
741　concentrations, and consequent atmospheric chemistry, and this data has already been
742　incorporated in a new global iodide parameterisation (Sherwen et al. 2019).
743
744　The large scale latitudinal trends observed in the Indian Ocean and Indian sector of the
745　Southern Ocean are similar to those in other ocean basins (Chance et al. 2014). We have used
746　a state-of-the-art global iodine cycling model (Wadley et al. 2020) to explore the controls on
747　the sea-surface iodide distribution in the Indian Ocean basin. Model sensitivity tests indicate
748　that sea surface iodide is likely to be a function of vertical mixing and the seasonal cycle in
749　MLD, the rate of iodide production, which is related to productivity and the I:C ratio, and – at
750　lower latitudes – iodide oxidation in the mixed layer. These factors interact in a non-linear
751　manner.
752
753　At subtropical latitudes, the latitudinal and temperature dependency of iodide is steeper than
754　in other ocean basins. Therefore, using global scale relationships with SST (e.g. (MacDonald
755　et al. 2014)) to predict regional scale iodide concentrations for the Indian Ocean will be
756　subject to biases. Exploration of this basin scale difference using the model indicates that it is
757　driven by differences in biological productivity at subtropical latitudes.
758
759　Exceptionally high iodide concentrations were observed at a small number of stations in the
760　northern Indian Ocean. Such high concentrations are rare, but have been reported previously
761　in low oxygen subsurface waters (Farrenkopf and Luther 2002), and more recently, in surface
762　waters above the Peruvian and Mexican oxygen deficient zones (Cutter et al. 2018; Moriyasu
763　et al. 2020). In all cases, the excess iodide is suggested to be sedimentary in origin, raising
764　the possibility that processes at the sea floor could influence air-sea interactions, should that
765　water reach the sea surface. Although such iodide 'hot-spots' are unlikely to have significant
766　impact on a global or regional scale, it is possible they may impact on local scale air-sea
767　exchange processes involving iodine. Their existence also means care must be taken to
768　ensure iodide concentrations used to generate parameterisations are representative of the
769　entire study area.
770
771　Marine iodine cycling is anticipated to be affected by global change, with consequent impacts
772　on atmospheric chemistry. The Indian Ocean basin is subject to a number of specific
773　pressures with potential to affect iodine cycling. Despite the empirical relationship between
774　SSI and SST, changes in vertical mixing as a result of the Indian Ocean warming may in fact
775　reduce mixed layer iodide concentrations. Meanwhile, changes to biological processes as a
776　result of anthropogenic nutrient inputs, ocean deoxygenation and changes in heat distribution

777   are likely to impact iodide production and loss processes. Such changes will in turn impact
778   ozone deposition and iodine emission from the sea surface.

Author contributions

LT, AS, AKS and AM collected seawater samples during the three research cruises; LT and RJC analysed samples for iodine speciation; AS, AKS and RR provided supporting biogeochemical measurements; RC and PS provided insight regarding physical oceanography in the study area; DS and MW performed the iodine modelling described in Section 4; RJC and LT interpreted the data and wrote the manuscript with input from TDJ and MW, other authors also provided comments on the manuscript; LJC, TDJ, AM and RJC conceived the study.

Conflict of Interest

The authors declare no competing interests.

References

Aksenov, Yevgeny, Sheldon Bacon, Andrew C. Coward, and A. J. George Nurser. 2010. 'The North Atlantic inflow to the Arctic Ocean: High-resolution model study', Journal of Marine Systems, 79: 1-22.

Allan, J. D., P. I. Williams, J. Najera, J. D. Whitehead, M. J. Flynn, J. W. Taylor, D. Liu, E. Darbyshire, L. J. Carpenter, R. Chance, S. J. Andrews, S. C. Hackenberg, and G. McFiggans. 2015. 'Iodine observed in new particle formation events in the Arctic atmosphere during ACCACIA', Atmospheric Chemistry and Physics (Print), 15: 5599-609.

Behrenfeld, Michael, and Paul Falkowski. 1997. 'Behrenfeld MJ, Falkowski PG. Photosynthetic rates derived from satellite-based chlorophyll concentration. Limnol Oceanogr 41: 1-20', Limnology and Oceanography, 42: 1-20.

Bluhm, K., P. L. Croot, O. Huhn, G. Rohardt, and K. Lochte. 2011. 'Distribution of iodide and iodate in the Atlantic sector of the southern ocean during austral summer', Deep-Sea Research Part II-Topical Studies in Oceanography, 58: 2733-48.

Bluhm, K., P. Croot, K. Wuttig, and K. Lochte. 2010. 'Transformation of iodate to iodide in marine phytoplankton driven by cell senescence', Aquatic Biology, 11: 1-15.

Campos, M.L.A.M. 1997. 'New approach to evaluating dissolved iodine speciation in natural waters using cathodic stripping voltammetry and a storage study for preserving iodine species', Marine Chemistry, 57: 107-17.

Campos, M.L.A.M., A. M. Farrenkopf, T. D. Jickells, and G. W. Luther. 1996. 'A comparison of dissolved iodine cycling at the Bermuda Atlantic Time-Series station and Hawaii Ocean Time-Series Station', Deep-Sea Research Part II: Topical Studies in Oceanography, 43: 455-66.

Campos, M.L.A.M., R. Sanders, and T. Jickells. 1999. 'The dissolved iodate and iodide distribution in the South Atlantic from the Weddell Sea to Brazil', Marine Chemistry, 65: 167-75.

Carpenter, L. J., S. M. MacDonald, M. D. Shaw, R. Kumar, R. W. Saunders, R. Parthipan, J. Wilson, and J. M. C. Plane. 2013. 'Atmospheric iodine levels influenced by sea surface emissions of inorganic iodine', Nature Geoscience, 6: 108-11.

Chance, R., A. R. Baker, L. Carpenter, and T. D. Jickells. 2014. 'The distribution of iodide at the sea surface', Environmental Science-Processes & Impacts, 16: 1841-59.

Chance, R.J., L. Tinel, T. Sherwen, A. Baker, T. Bell, J. Brindle, M.L.A.M. Campos, P. Croot, H. Ducklow, P. He, B. Hoogakker, F.E. Hopkins, C. Hughes, T. Jickells, D. Loades, D.A. Reyes Macaya, A.S. Mahajan, G. Malin, D.P. Phillips, A.K. Sinha, A. Sarkar, I.J. Roberts, R. Roy, X. Song, H.A. Winklebauer, K. Wuttig, M. Yang, P. Zhou, and L.J. Carpenter. 2019. "Global sea-surface iodide observations, 1967-2018." In. British Oceanographic Data Centre - Natural Environment Research Council, UK.

Chance, R.J., L. Tinel, T. Sherwen, A.R. Baker, T. Bell, J. Brindle, M.L.A.M. Campos, P. Croot, H. Ducklow, P. He, F. Hopkins, B. Hoogakker, C. Hughes, T.D. Jickells, D. Loades, D.A.R. Macaya, A.S. Mahajan, G. Malin, D. Phillips, I. Roberts, R. Roy, A. Sarkar, A.K. Sinha, X. Song, H. Winkelbauer, K. Wuttig, M. Yang, Peng Zhou, and L.J. Carpenter. 2019. 'Global sea-surface iodide observations, 1967-2018', Scientific Data, 6: 286.

Chance, Rosie, Keith Weston, Alex R. Baker, Claire Hughes, Gill Malin, Lucy Carpenter, Michael P. Meredith, Andrew Clarke, Timothy D. Jickells, Paul Mann, and Helen Rossetti. 2010. 'Seasonal and interannual variation of dissolved iodine speciation at a coastal Antarctic site', Marine Chemistry, 118: 171-81.

Cuevas, C. A., N. Maffezzoli, J. P. Corella, A. Spolaor, P. Vallelonga, H. A. Kjaer, M. Simonsen, M. Winstrup, B. Vinther, C. Horvat, R. P. Fernandez, D. Kinnison, J. F. Lamarque, C. Barbante, and A. Saiz-Lopez. 2018. 'Rapid increase in atmospheric iodine levels in the North Atlantic since the mid-20th century', Nature Communications, 9: 6.

Cutter, G. A., J. G. Moffett, M. C. Nielsdottir, and V. Sanial. 2018. 'Multiple oxidation state trace elements in suboxic waters off Peru: In situ redox processes and advective/diffusive horizontal transport', Marine Chemistry, 201: 77-89.

Ducklow, H. W., M. R. Stukel, R. Eveleth, S. C. Doney, T. Jickells, O. Schofield, A. R. Baker, J. Brindle, R. Chance, and N. Cassar. 2018. 'Spring-summer net community production, new production, particle export and related water column biogeochemical processes in the marginal sea ice zone of the Western Antarctic Peninsula 2012-2014', Philosophical Transactions of the Royal Society a-Mathematical Physical and Engineering Sciences, 376: 15.

Edwards, A., and V. W. Truesdale. 1997. 'Regeneration of inorganic iodine species in Loch Etive, a natural leaky incubator', Estuarine Coastal and Shelf Science, 45: 357-66.

Elderfield, H., and V. W. Truesdale. 1980. 'On the biophilic nature of iodine in seawater', Earth and Planetary Science Letters, 50: 105-14.

Farrenkopf, A. M., and G. W. Luther. 2002. 'Iodine chemistry reflects productivity and denitrification in the Arabian Sea: evidence for flux of dissolved species from sediments of western India into the OMZ', Deep-Sea Research Part II-Topical Studies in Oceanography, 49: 2303-18.

Farrenkopf, A. M., G. W. Luther, V. W. Truesdale, and C. H. Van Der Weijden. 1997. 'Sub-surface iodide maxima: evidence for biologically catalyzed redox cycling in Arabian Sea OMZ during the SW intermonsoon', Deep Sea Research Part II: Topical Studies in Oceanography, 44: 1391-409.

Ganzeveld, L., D. Helmig, C. W. Fairall, J. Hare, and A. Pozzer. 2009. 'Atmosphere-ocean ozone exchange: A global modeling study of biogeochemical, atmospheric, and waterside turbulence dependencies', Global Biogeochemical Cycles, 23.

Ghose, N. C., K. Das, and D. Saha. 2003. 'Distribution of iodine in soil-water system in the Gandak basin, Bihar', Journal of the Geological Society of India, 62: 91-98.

Gilfedder, B. S., M. Petri, and H. Biester. 2007. 'Iodine speciation in rain and snow: Implications for the atmospheric iodine sink', Journal of Geophysical Research-Atmospheres, 112: 7.

Grand, Maxime M., Christopher I. Measures, Mariko Hatta, William T. Hiscock, William M. Landing, Peter L. Morton, Clifton S. Buck, Pamela M. Barrett, and Joseph A. Resing. 2015. 'Dissolved Fe and Al in the upper 1000 m of the eastern Indian Ocean: A high-resolution transect along 95°E from the Antarctic margin to the Bay of Bengal', Global Biogeochemical Cycles, 29: 375-96.

Hardacre, C., O. Wild, and L. Emberson. 2015. 'An evaluation of ozone dry deposition in global scale chemistry climate models', Atmospheric Chemistry and Physics (Print), 15: 6419-36.

Hardisty, D. S., T. J. Horner, S. D. Wankel, J. Blusztajn, and S. G. Nielsen. 2020. 'Experimental observations of marine iodide oxidation using a novel sparge-interface MC-ICP-MS technique', Chemical Geology, 532: 119360.

Hou, Xiaolin, Ala Aldahan, Sven P. Nielsen, Goran Possnert, Hartmut Nies, and Jim Hedfors. 2007. 'Speciation of I-129 and I-127 in seawater and implications for sources and transport pathways in the North Sea', Environmental Science & Technology, 41: 5993-99.

910 Hughes, C., E. Barton, H. Hepach, R. Chance, M. Pickering, and K. Hogg. 2020. 'Iodate
911   production in marine ammonium-oxidising bacteria', *Manuscript to be submitted to*
912   *Global Biogeochemical Cycles*.
913 Jickells, T. D., S. S. Boyd, and A. H. Knap. 1988. 'Iodine cycling in the Sargasso Sea and the
914   Bermuda Inshore waters', Marine Chemistry, 24: 61-82.
915 Johannessen, T., and E. Dahl. 1996. 'Declines in oxygen concentrations along the Norwegian
916   Skagerrak coast, 1927-1993: A signal of ecosystem changes due to eutrophication?',
917   Limnology and Oceanography, 41: 766-78.
918 Longhurst, A.R. 1998. Ecological geography of the sea (Academic: San Diego).
919 Lu, Wanyi, Andy Ridgwell, Ellen Thomas, Dalton S. Hardisty, Genming Luo, Thomas J.
920   Algeo, Matthew R. Saltzman, Benjamin C. Gill, Yanan Shen, Hong-Fei Ling, Cole T.
921   Edwards, Michael T. Whalen, Xiaoli Zhou, Kristina M. Gutchess, Li Jin, Rosalind E.
922   M. Rickaby, Hugh C. Jenkyns, Timothy W. Lyons, Timothy M. Lenton, Lee R. Kump,
923   and Zunli Lu. 2018. 'Late inception of a resiliently oxygenated upper ocean', Science:
924   eaar5372.
925 Luther, G. W., C. B. Swartz, and W. J. Ullman. 1988. 'Direct determination of iodide in
926   seawater by cathodic stripping square-wave voltammetry', Analytical Chemistry, 60:
927   1721-24.
928 MacDonald, S. M., J. C. Gómez Martín, R. Chance, S. Warriner, A. Saiz-Lopez, L. J.
929   Carpenter, and J. M. C Plane. 2014. 'A laboratory characterisation of inorganic iodine
930   emissions from the sea surface: dependence on oceanic variables and parameterisation
931   for global modelling', Atmospheric Chemistry and Physics, 14: 5841-52.
932 Mahajan, Anoop S., Liselotte Tinel, Shrivardhan Hulswar, Carlos A. Cuevas, Shanshan Wang,
933   Sachin Ghude, Ravidas K. Naik, Rajani K. Mishra, P. Sabu, Amit Sarkar, N.
934   Anilkumar, and Alfonso Saiz Lopez. 2019. 'Observations of iodine oxide in the Indian
935   Ocean marine boundary layer: A transect from the tropics to the high latitudes',
936   Atmospheric Environment: X, 1: 100016.
937 McFiggans, G., H. Coe, R. Burgess, J. Allan, M. Cubison, M. R. Alfarra, R. Saunders, A. Saiz-
938   Lopez, J. M. C. Plane, D. J. Wevill, L. J. Carpenter, A. R. Rickard, and P. S. Monks.
939   2004. 'Direct evidence for coastal iodine particles from Laminaria macroalgae - linkage
940   to emissions of molecular iodine', Atmospheric Chemistry and Physics, 4: 701-13.
941 Moran, Jean E., Sarah D. Oktay, and Peter H. Santschi. 2002. 'Sources of iodine and iodine
942   129 in rivers', Water Resources Research, 38: 24-1-24-10.
943 Moriyasu, Rintaro, Zachary C. Evans, Kenneth M. Bolster, Dalton S. Hardisty, and James W.
944   Moffett. 2020. 'The Distribution and Redox Speciation of Iodine in the Eastern Tropical
945   North Pacific Ocean', Global Biogeochemical Cycles, 34: e2019GB006302.
946 Nakayama, E., T. Kimoto, K. Isshiki, Y. Sohrin, and S. Okazaki. 1989. 'Determination and
947   distribution of iodide-iodine and total-iodine in the north Pacific ocean by using a new
948   automated electrochemical method', Marine Chemistry, 27: 105-16.
949 Naqvi, S. W. A., D. A. Jayakumar, P. V. Narvekar, H. Naik, V. V. S. S. Sarma, W. D'Souza,
950   S. Joseph, and M. D. George. 2000. 'Increased marine production of N2O due to
951   intensifying anoxia on the Indian continental shelf', Nature, 408: 346.
952 Orsi, Alejandro H., Thomas Whitworth, and Worth D. Nowlin. 1995. 'On the meridional extent
953   and fronts of the Antarctic Circumpolar Current', Deep Sea Research Part I:
954   Oceanographic Research Papers, 42: 641-73.
955 Prados-Roman, C., C. A. Cuevas, T. Hay, R. P. Fernandez, A. S. Mahajan, S. J. Royer, M.
956   Galí, R. Simó, J. Dachs, K. Großmann, D. E. Kinnison, J. F. Lamarque, and A. Saiz-
957   Lopez. 2015. 'Iodine oxide in the global marine boundary layer', Atmospheric
958   Chemistry and Physics (Print), 15: 583-93.

959 Sadasivan, S., and S. J. S. Anand. 1979. 'Chlorine, bromine and iodine in monsoon rains in
960   India', Tellus, 31: 290-94.
961 Sarwar, G., D. W. Kang, K. Foley, D. Schwede, B. Gantt, and R. Mathur. 2016. 'Technical
962   note: Examining ozone deposition over seawater', Atmospheric Environment, 141: 255-
963   62.
964 Schlitzer, R. 2014. "Ocean Data View." In.: http://odv.awi.de.
965 Schwehr, K. A., and P. H. Santschi. 2003. 'Sensitive determination of iodine species, including
966   organo-iodine, for freshwater and seawater samples using high performance liquid
967   chromatography and spectrophotometric detection', Analytica Chimica Acta, 482: 59-
968   71.
969 Sherwen, T., M. J. Evans, R. Sommariva, L. D. J. Hollis, S. M. Ball, P. S. Monks, C. Reed, L.
970   J. Carpenter, J. D. Lee, G. Forster, B. Bandy, C. E. Reeves, and W. J. Bloss. 2017.
971   'Effects of halogens on European air-quality', Faraday Discussions, 200: 75-100.
972 Sherwen, T.S., L. Tinel, R. Chance, L.J. Carpenter, and M.J. Evans. 2019. 'Re-approaching
973   global iodine emissions: A novel parameterisation for sea-surface iodide concentrations
974   using a machine learning approach. In prep.'.
975 Truesdale, V. W. 1978. 'Iodine in inshore and off-shore marine waters', Marine Chemistry, 6:
976   1-13.
977 Truesdale, V. W., A. J. Bale, and E. M. S. Woodward. 2000. 'The meridional distribution of
978   dissolved iodine in near-surface waters of the Atlantic Ocean', Progress in
979   Oceanography, 45: 387-400.
980 Truesdale, V. W., D. S. Danielssen, and T. J. Waite. 2003. 'Summer and winter distributions
981   of dissolved iodine in the Skagerrak', Estuarine Coastal and Shelf Science, 57: 701-13.
982 Truesdale, V. W., and C. P. Spencer. 1974. 'Studies on the determination of inorganic iodine
983   in seawater', Marine Chemistry, 2: 33-47.
984 Tsunogai, S. 1971. 'Iodine in the deep water of the ocean', Deep-Sea Research, 18: 913-19.
985 Tsunogai, S., and T. Henmi. 1971. 'Iodine in the surface water of the Pacific Ocean', Journal
986   of the Oceanographical Society of Japan, 27: 67-72.
987 Vinayachandran, P. N., Adrian J. Matthews, K. Vijay Kumar, Alejandra Sanchez-Franks, V.
988   Thushara, Jenson George, V. Vijith, Benjamin G. M. Webber, Bastien Y. Queste,
989   Rajdeep Roy, Amit Sarkar, Dariusz B. Baranowski, G. S. Bhat, Nicholas P. Klingaman,
990   Simon C. Peatman, C. Parida, Karen J. Heywood, Robert Hall, Brian King, Elizabeth
991   C. Kent, Anoop A. Nayak, C. P. Neema, P. Amol, A. Lotliker, A. Kankonkar, D. G.
992   Gracias, S. Vernekar, A. C. D'Souza, G. Valluvan, Shrikant M. Pargaonkar, K. Dinesh,
993   Jack Giddings, and Manoj Joshi. 2018. 'BoBBLE: Ocean–Atmosphere Interaction and
994   Its Impact on the South Asian Monsoon', Bulletin of the American Meteorological
995   Society, 99: 1569-87.
996 Wadley, M.R., D.P. Stevens, T.D. Jickells, C. Hughes, A.R. Baker, R.J. Chance, H. Hepach,
997   L. Tinel, and L.J. Carpenter. 2020. 'A Global Model for Iodine Speciation in the Upper
998   Ocean', Global Biogeochemical Cycles, Resubmitted manuscript.
999 Waite, T. J., V. W. Truesdale, and J. Olafsson. 2006. 'The distribution of dissolved inorganic
1000   iodine in the seas around Iceland', Marine Chemistry, 101: 54-67.
1001 Wang, F., A. Saiz-Lopez, A. S. Mahajan, J. C. Gómez Martín, D. Armstrong, M. Lemes, T.
1002   Hay, and C. Prados-Roman. 2014. 'Enhanced production of oxidised mercury over the
1003   tropical Pacific Ocean: a key missing oxidation pathway', Atmospheric Chemistry and
1004   Physics (Print), 14: 1323-35.
1005 Wong, G. T. F. 2001. 'Coupling iodine speciation to primary, regenerated or "new" production:
1006   a re-evaluation', Deep-Sea Research Part I-Oceanographic Research Papers, 48: 1459-
1007   76.

1008   Wong, G. T. F., and X. H. Cheng. 1998. 'Dissolved organic iodine in marine waters:
1009   Determination, occurrence and analytical implications', Marine Chemistry, 59: 271-81.
1010   Wong, G. T. F., and L. S. Zhang. 2003. 'Geochemical dynamics of iodine in marginal seas: the
1011   southern East China Sea', Deep-Sea Research Part II-Topical Studies in Oceanography,
1012   50: 1147-62.
1013   Zic, V., M. Caric, and I. Ciglenecki. 2013. 'The impact of natural water column mixing on
1014   iodine and nutrient speciation in a eutrophic anchialine pond (Rogoznica Lake,
1015   Croatia)', Estuarine Coastal and Shelf Science, 133: 260-72.
1016

Figures
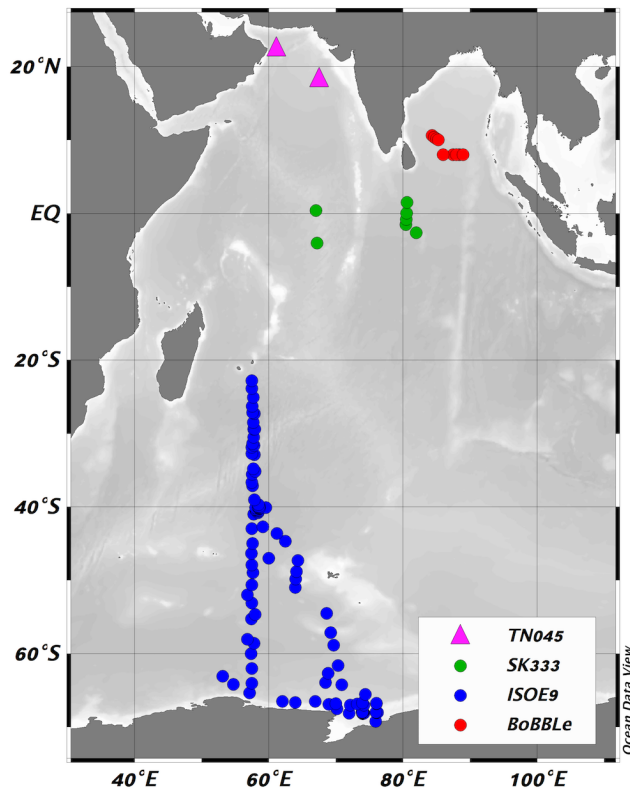
1019
1020
1021 Figure 1. Locations of new sea surface iodide observations made during this work, coloured
1022 according to cruise (green – SK333, red – BoBBLe, blue – ISOE9) and previous observations
1023 from the region made by Farrenkopf et al., 2002, and included in the compilation of Chance et
1024 al., 2014 (pink triangles). Figure produced using Ocean Data View (Schlitzer 2014).
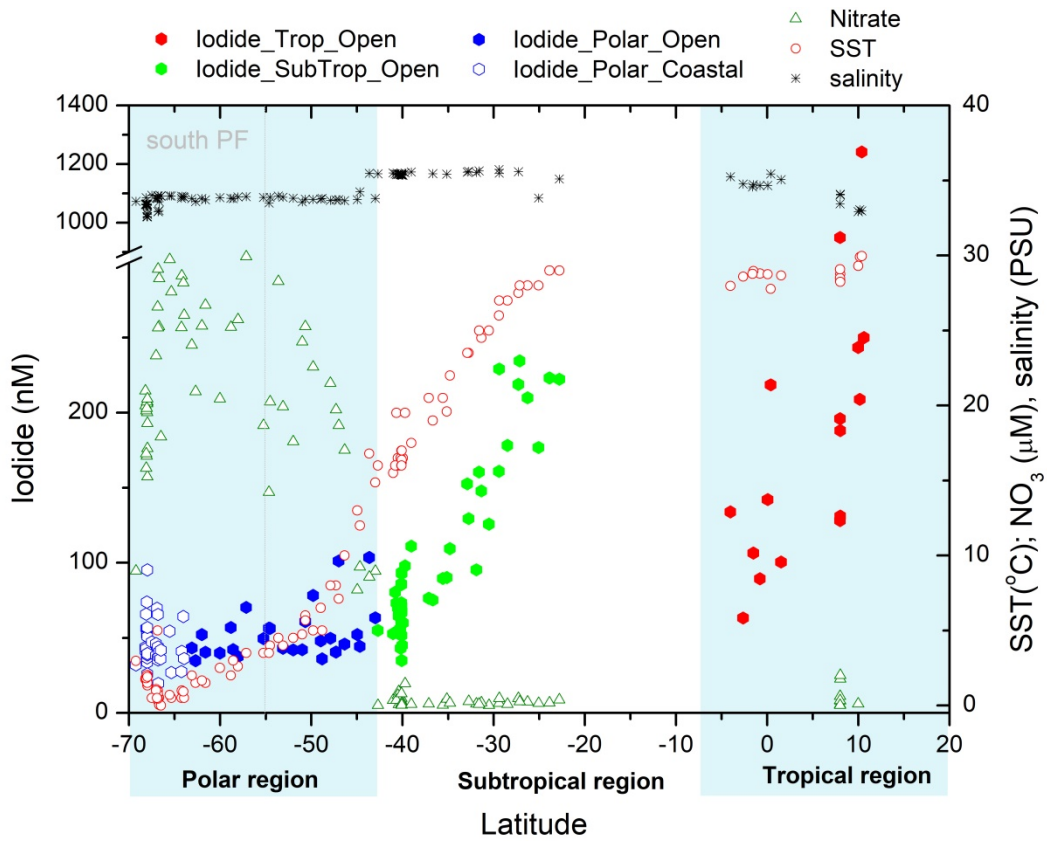
Figure 2. Latitudinal variation of surface iodide concentrations in nM observed in the open
Indian and Southern Ocean (●) and in the coastal Southern Ocean (o) compared to the
observed sea surface temperature (˚C), salinity (PSU) and nitrate concentrations (µM). Boxes
indicate the three different oceanographic regimes considered in the text. The dotted grey line
indicates the position of the Polar Front (PF).
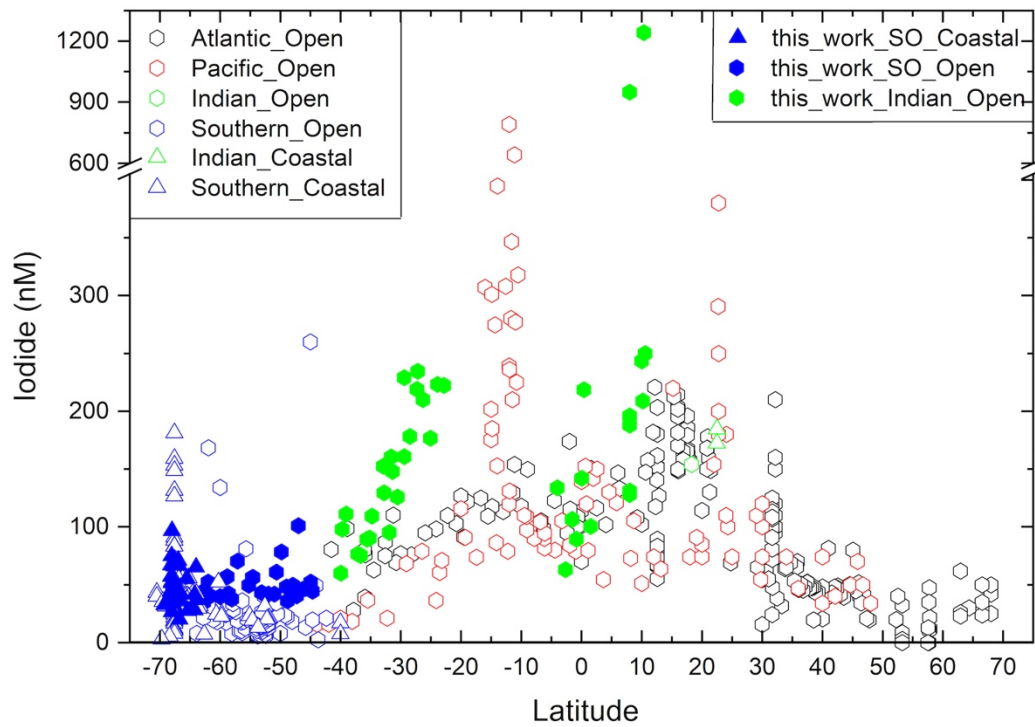
Figure 3. Latitudinal variation of sea surface iodide concentrations in the Indian (green) and Indian sector of the Southern Ocean (SO; blue), compared to other ocean basins (Atlantic – black, Pacific – red). New observations made as part of this work are shown with filled symbols, while other values (see compilation of (Chance, Tinel, Sherwen, Baker, Bell, Brindle, Campos, Croot, Ducklow, He, Hopkins, et al. 2019)) are shown in hollow symbols. Division between ocean basins follows the borders proposed by the World Ocean Circulation Experiment (https://www.nodc.noaa.gov/woce/woce_v3/wocedata_1/woce-uot/summary/bound.htm), and (Orsi, Whitworth, and Nowlin 1995) for the Southern Ocean.

1044
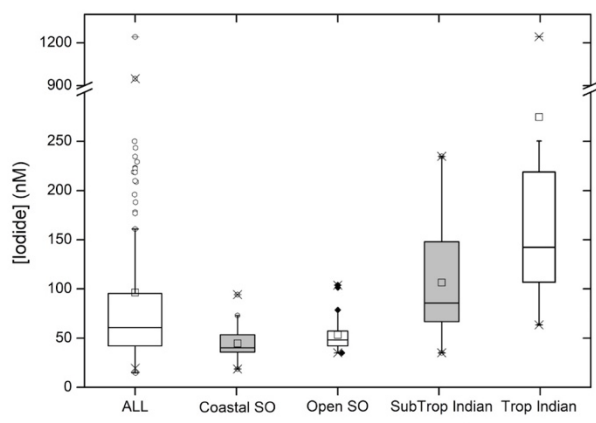
1045
1046
1047 Figure 4. Box and Whisker plot showing descriptive statistics for the entire data set
1048 ('ALL'; n=127) and sub-divided into the following regions: polar coastal waters
1049 ('Coastal SO'; n=38), open waters of the Southern Ocean ('Open SO'; n=27), the Indian
1050 Ocean subtropical convergence zone and southern subtropical gyre ('SubTrop Indian';
1051 n=46 and the tropical Indian Ocean ('Trop Indian'; n=16). See main text for more
1052 detailed descriptions of these categories. Centre lines show the medians; squares are
1053 the means; box limits indicate the 25th and 75th percentiles; whiskers extend 1.5 times
1054 the interquartile range from the 25th and 75th percentiles, outliers are represented by
1055 dots; crosses represent 1st and 99th percentiles; width of the boxes is proportional to the
1056 square root of the sample size.
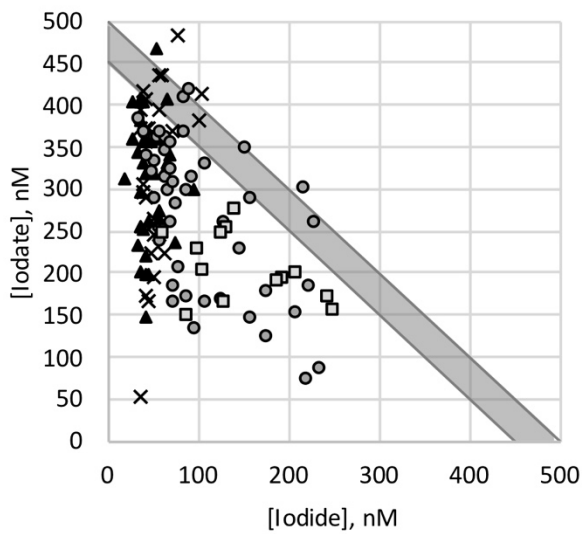
Figure 5. Sea surface iodate concentrations plotted against iodide concentrations, for samples from polar coastal waters (▲), open waters of the Southern Ocean (✖), the Indian Ocean subtropical convergence zone and southern subtropical gyre (○) and the tropical Indian Ocean (□). Grey line shows 1:1 relationship, assuming a total inorganic iodine concentration of 450 to 500 nM (Chance et al. 2014). Note for clarity two samples with very high iodide concentrations not shown.
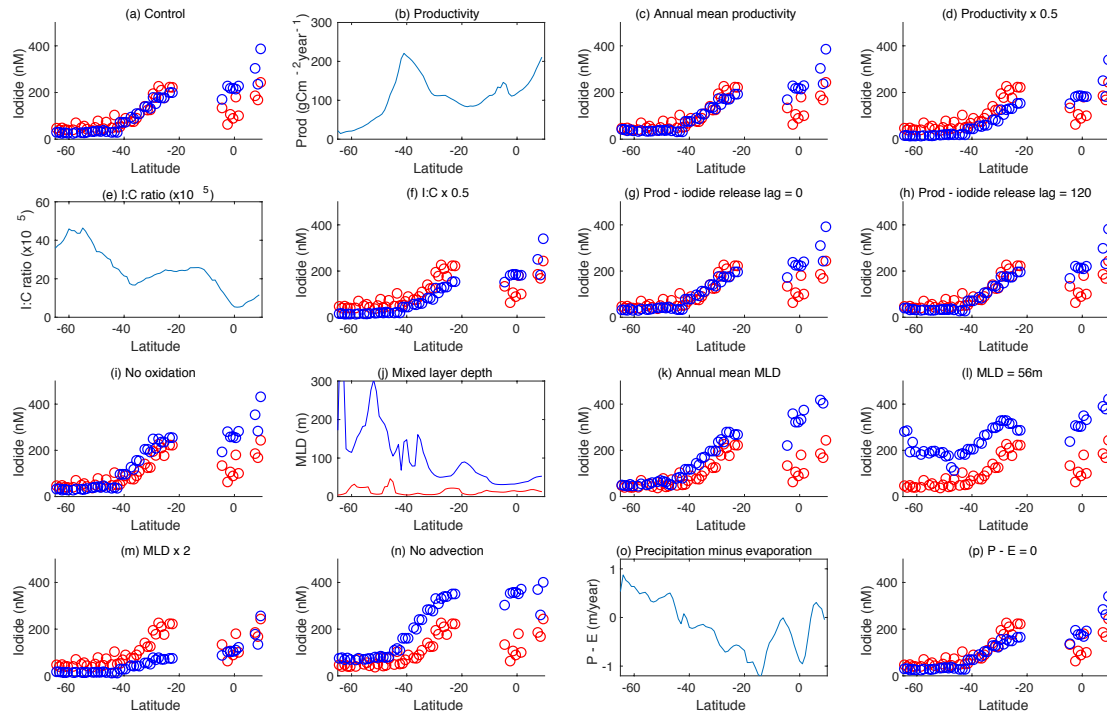
1066
Figure 6. Results from model process sensitivity experiments. (a) Observed (red) and model
(blue) iodide concentrations as a function of latitude, in the Indian Ocean and the Indian
sector of the Southern Ocean along a section at 60°E (note observed iodide over 500nM have
been excluded here) (b) observed primary productivity (Behrenfeld and Falkowski 1997) as a
function of latitude, (c) iodide with the seasonal cycle of productivity replaced with the
annual mean, (d) iodide with seasonal productivity halved, (e) the model I:C ratio, (f) iodide
with the model I:C ratio halved, (g) iodide with iodide release from plankton at the same time
as carbon assimilation, (h) iodide with iodide release from plankton lagged 120 days from
carbon assimilation, (i) no mixed layer oxidation of iodide, (j) maximum (blue) and minimum
(red) mixed layer depth from the OCCAM model (Aksenov et al., 2010) as a function of
latitude, (k) iodide with the seasonal cycle of mixed layer depth replaced with the annual
mean, (l) iodide with the seasonal cycle of mixed layer depth replaced by the constant global
mean of 56m, (m) seasonal MLD doubled, (n) no vertical or horizontal advection, (o) P-E
from the OCCAM model (Aksenov et al. 2010) as a function of latitude, (p) P-E set to zero.
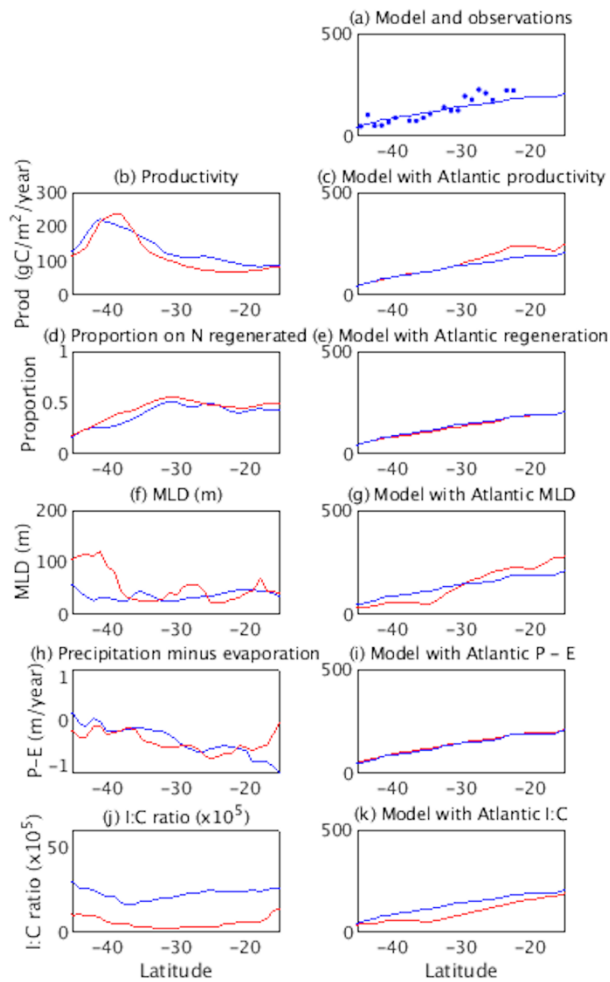
Figure 7. Impact of imposing Atlantic forcings in the Indian Ocean basin in the iodine cycling model. Plots are annual mean iodide for 57°E in the Indian Ocean. (a) observed (dots) and modelled (line) iodide, in nM (b,d,f,h, j) latitudinal sections for each process-related quantity for the Indian (blue) and Atlantic (red) Oceans, (c,e,g,i, k) corresponding latitudinal sections of iodide for control (blue) and Atlantic forcing imposed over the Indian basin (red).

1089 **Tables**
1090
1091 Table 1. Regression parameters for relationships between iodide (in nM) and latitude, SST
1092 and nitrate concentration. For each variable, top row gives results of Pearsons Product-
1093 Moment correlation (parametric) and bottom row gives results of Spearmans rank correlation
1094 (non-parametric). Statistically significant ($p < 5\%$) correlations are shown in bold. *Two
1095 extremely high iodide concentrations in tropical sub-set excluded from correlation analysis.
1096

| Independent variable	R^2 ρ_s	slope -	intercept -	p p
|latitude|				
All data	0.24	-3.4	251	**5 x 10⁻⁹**
	-0.74	-	-	**0**
Sub-tropical	0.86	-9.5	449	**3 x 10⁻²⁰**
	-0.83	-	-	**1.1 x 10⁻¹²**
Southern Ocean	0.10	-0.64	87	**0.01**
	-0.21	-	-	**9.6 x 10⁻³**
*Tropical**	0.39	9.2	109	**0.02**
	0.59	-	-	**1.7 x 10⁻²**
Chance et al., 2014	0.40	-2.7	200	**<0.05**
	-0.65	-	-	**<0.05**
SST (ºC)				
All data	0.26	5.7	21	**1 x 10⁻⁹**
	0.81	-	-	**0**
Sub-tropical	0.89	11.8	-130	**2 x 10⁻²²**
	0.87	-	-	**6.7 x 10⁻¹⁵**
Southern Ocean	0.15	1.8	43	**0.002**
	0.35	-	-	**4.2 x 10⁻³**
*Tropical**	0.14	37	901	0.2
	0.42	-	-	0.14
Chance et al., 2014	0.52	5.7	4	**<0.05**
	0.72	-	-	**<0.05**
[Nitrate], µM				
All data	0.17	-3.9	136	**3 x 10⁻⁵**
	-0.58	-	-	**1.6 x 10⁻¹⁰**
Sub-tropical	0.004	-13	118	0.7
	-0.02	-	-	0.93
Southern Ocean	0.03	-0.53	61	0.2
	-0.13	-	-	0.34
Tropical (n=5)	0.21	-31	195	0.4
	-0.14	-	-	0.79
Chance et al., 2014	0.36	-5.2	125	**<0.05**
	-0.73	-	-	**<0.05**

1097

Supplementary Information
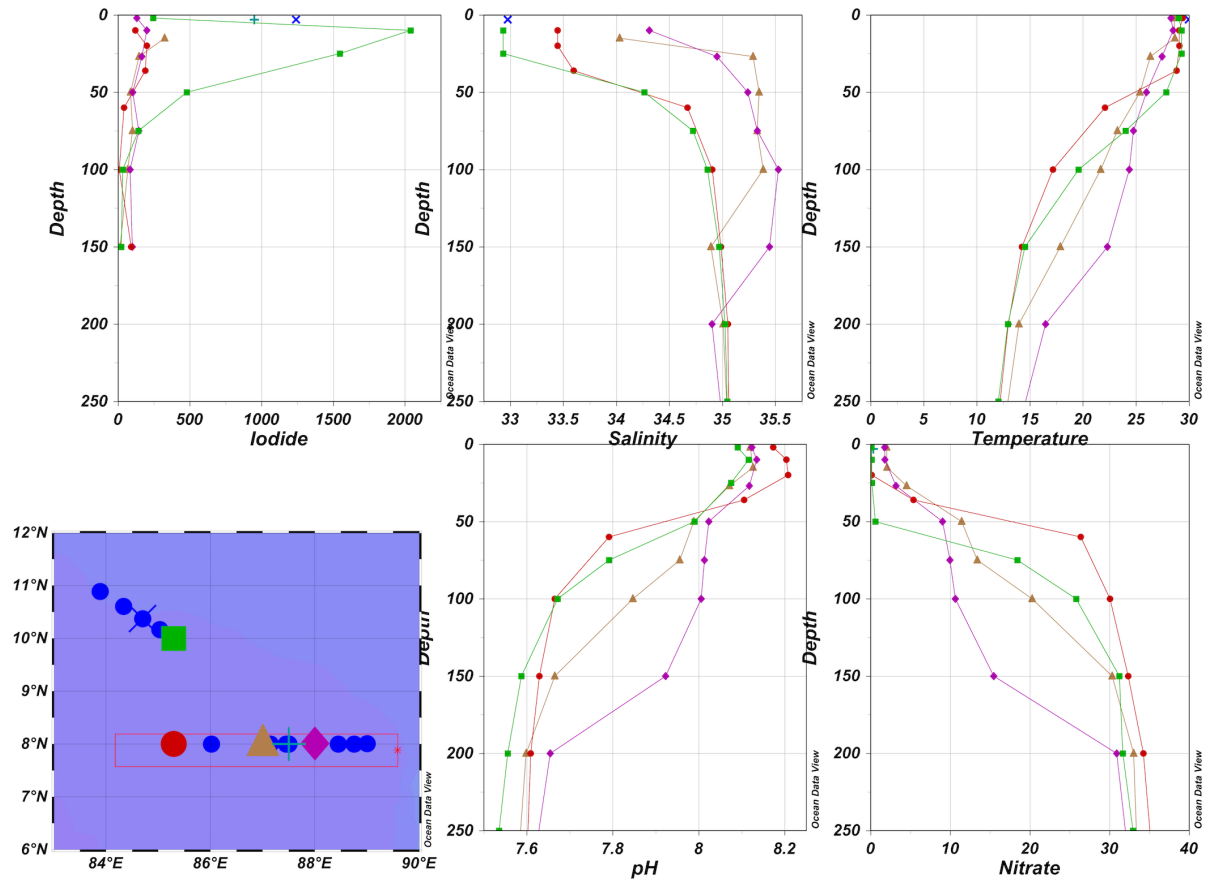
Figure S1. Selected depth profile data from the BoBBLe cruise in the Bay of Bengal, showing exceptionally high surface and subsurface iodide concentrations. Station AR shown in green squares, underway samples BS3 and BS8 shown by blue cross and green plus sign. Note the high salinity core of Summer Monsoon Current (SMC) evident in stations with purple & brown symbols. Figure prepared using Ocean Data View (Schlitzer 2014).
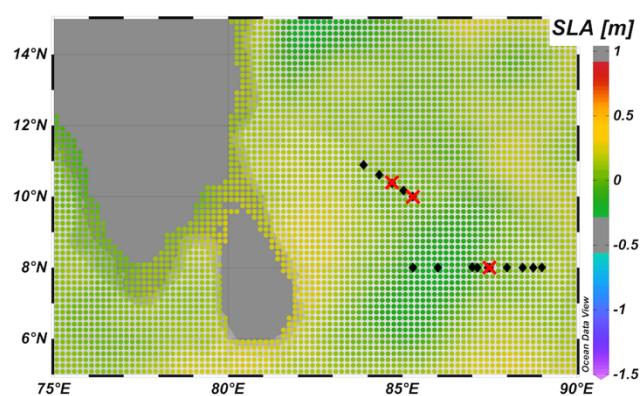
10
11

12
13
14
15 Figure S2. Sea surface height anomaly (SLA, m) for 26-30 June 2016 and BoBBLe station
16 positions, with high iodide stations indicated by red crosses. Green areas show negative sea
17 level anomalies, where upwelling is taking place, indicative of Sri Lanka Dome area. Dataset
18 (Zlotnicki, Qu, and Willis 2016) accessed [2017-01-21] at https://doi.org/10.5067/SLREF-
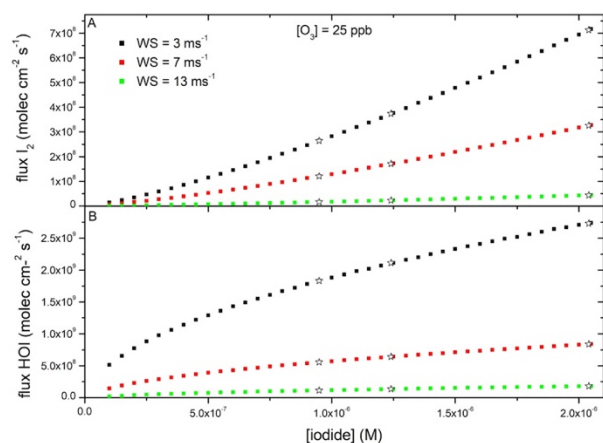19 CDRV1. Figure prepared using Ocean Data View (Schlitzer 2014).

Figure S3: Predicted fluxes for HOI and I₂ emissions (molecules cm⁻² s⁻¹) as a function of the aqueous iodide concentration (M) for a fixed ozone concentration of 25 ppb and three different wind speeds (black: 3 ms⁻¹, red: 7 ms⁻¹, green: 13 ms⁻¹), calculated using the parametrisation in (Carpenter et al. 2013). The stars symbols show the predicted fluxes for the high (>600nM) iodide concentrations measured in the tropical Indian Ocean during the BoBBLe cruise.

Table S1. Gradients of sea surface iodide concentrations against latitude and sea surface temperature (SST) for open ocean subtropical waters (defined by province) of the global ocean basins. Iodide data from (Chance, Tinel, Sherwen, Baker, Bell, Brindle, Campos, Croot, Ducklow, He, Hopkins, et al. 2019) and sea surface temperatures from the World Ocean Atlas 2013 (Locarnini et al. 2013).

		[I⁻] vs |Latitude|		[I⁻] vs. SST		Modal month	% Frequency of modal month
	n	slope	R^2	slope	R^2		
North Atlantic	123	-3.5	0.40	12.2	0.47	11	39
South Atlantic	27	-2.2	0.60	6.3	0.60	10	70
North Pacific	24	-3.5	0.06	9.9	0.24	3	38
South Pacific	27	-14.3	0.40	6.6	0.01	11	37
South pacific ex. Cutter et al	10	-2.8	0.59	6.7	0.65	1	90
South Indian	46	-9.5	0.85	13.3	0.84	1	67
South Indian, modelled	--	-5.5	0.99	--	--	--	--

References

Carpenter, L. J., S. M. MacDonald, M. D. Shaw, R. Kumar, R. W. Saunders, R. Parthipan, J. Wilson, and J. M. C. Plane. 2013. 'Atmospheric iodine levels influenced by sea surface emissions of inorganic iodine', Nature Geoscience, 6: 108-11.

Chance, R.J., L. Tinel, T. Sherwen, A. Baker, T. Bell, J. Brindle, M.L.A.M. Campos, P. Croot, H. Ducklow, P. He, B. Hoogakker, F.E. Hopkins, C. Hughes, T. Jickells, D. Loades, D.A. Reyes Macaya, A.S. Mahajan, G. Malin, D.P. Phillips, A.K. Sinha, A. Sarkar, I.J. Roberts, R. Roy, X. Song, H.A. Winklebauer, K. Wuttig, M. Yang, P. Zhou, and L.J. Carpenter. 2019. "Global sea-surface iodide observations, 1967-2018." In. British Oceanographic Data Centre - Natural Environment Research Council, UK.

Locarnini, R. A., A.V. Mishonov, J.I. Antonov, T.P. Boyer, H.E. Garcia, O.K. Baranova, M.M. Zweng, C.R. Paver, J.R. Reagan, D.R. Johnson, M. Hamilton, and D. Seidov. 2013. "World Ocean Atlas 2013, Volume 1: Temperature." In, edited by S. Levitus and A. Mishonov, 40. Washington, D.C.: U.S. Government Printing Office.

Schlitzer, R. 2014. "Ocean Data View." In.: http://odv.awi.de.

Zlotnicki, V., Z. Qu, and J. Willis. 2016. "JPL MEaSUREs Gridded Sea Surface Height Anomalies Version 1609." In, edited by NASA Physical Oceanography DAAC. NASA Physical Oceanography DAAC.